Atmos. Chem. Phys., 16, 12567–12586, 2016
www.atmos-chem-phys.net/16/12567/2016/
doi:10.5194/acp-16-12567-2016

Atmospheric Chemistry and Physics Open Access EGU

Detection of Saharan dust and biomass burning events using near-real-time intensive aerosol optical properties in the north-western Mediterranean

Marina Ealo[1,2], Andrés Alastuey[1], Anna Ripoll[1], Noemí Pérez[1], María Cruz Minguillón[1], Xavier Querol[1], and Marco Pandolfi[1]

[1]Institute of Environmental Assessment and Water Research (IDAEA-CSIC), Barcelona, Spain
[2]Department of Astronomy and Meteorology, Faculty of Physics, University of Barcelona, Barcelona, Spain

Correspondence to: Marina Ealo (marina.ealo@idaea.csic.es)

Received: 3 November 2015 – Published in Atmos. Chem. Phys. Discuss.: 18 January 2016
Revised: 22 September 2016 – Accepted: 23 September 2016 – Published: 10 October 2016

Abstract. The study of Saharan dust events (SDEs) and biomass burning (BB) emissions are both topics of great scientific interest since they are frequent and important polluting scenarios affecting air quality and climate. The main aim of this work is evaluating the feasibility of using near-real-time in situ aerosol optical measurements for the detection of these atmospheric events in the western Mediterranean Basin (WMB). With this aim, intensive aerosol optical properties (SAE: scattering Ångström exponent, AAE: absorption Ångström exponent, SSAAE: single scattering albedo Ångström exponent and g: asymmetry parameter) were derived from multi-wavelength aerosol light scattering, hemispheric backscattering and absorption measurements performed at regional (Montseny; MSY, 720 m a.s.l.) and continental (Montsec; MSA, 1570 m a.s.l.) background sites in the WMB. A sensitivity study aiming at calibrating the measured intensive optical properties for SDEs and BB detection is presented and discussed.

The detection of SDEs by means of the SSAAE parameter and Ångström matrix (made up by SAE and AAE) depended on the altitude of the measurement station and on SDE intensity. At MSA (mountain-top site) SSAAE detected around 85 % of SDEs compared with 50 % at the MSY station, where pollution episodes dominated by fine anthropogenic particles frequently masked the effect of mineral dust on optical properties during less intense SDEs. Furthermore, an interesting feature of SSAAE was its capability to detect the presence of mineral dust after the end of SDEs. Thus, resuspension processes driven by summer regional atmospheric circulations and dry conditions after SDEs favoured the accumulation of mineral dust at regional level having important consequences for air quality. On average, SAE, AAE and g ranged between −0.7 and 1, 1.3 and 2.5 and 0.5 and 0.75 respectively during SDEs.

Based on the aethalometer model, BB contribution to equivalent black carbon (BC) accounted for 36 and 40 % at MSY and MSA respectively. Linear relationships were found between AAE and $\%BC_{bb}$, with AAE values reaching around 1.5 when $\%BC_{bb}$ was higher than 50 %. BB contribution to organic matter (OM) at MSY was around 30 %. Thus fossil fuel (FF) combustion sources showed important contributions to both BC and OM in the region under study. Results for OM source apportionment showed good agreement with simultaneous biomass burning organic aerosol (BBOA) and hydrocarbon-like organic aerosol (HOA) obtained by applying a positive matrix factorization model (PMF) to simultaneous Aerosol Chemical Speciation Monitor (ACSM) measurements. A wildfire episode was identified at MSY, showing AAE values up to 2 when daily BB contributions to BC and OM were 73 and 78 % respectively.

1 Introduction

Atmospheric aerosols play an important role in our environment, affecting air quality and health (Pope and Dockery, 2006) and contributing to the largest uncertainties to the total radiative forcing (IPCC, 2007, 2013). Aerosol affects climate by perturbation of the Earth's radiative budget, di-

rectly through absorption and scattering of solar and terrestrial radiation and indirectly by acting as cloud condensation nuclei (Twomey et al., 1984; Albrecht, 1989). Most particles scatter the sunlight, causing a net cooling at the top of the atmosphere (TOA), whereas black carbon (BC) absorbs solar radiation in the whole visible spectrum, thus causing a net warming at the TOA (Jacobson, 2001; Ramanathan and Carmichael, 2008; Bond et al., 2013). Absorbing particles can modify the radiation fluxes directly by absorption of shortwave solar radiation and semi-directly by modifying the temperature distribution of the atmosphere. Absorption in the UV range is important, since it may affect photochemistry, thus reducing tropospheric ozone concentration (Jacobson, 1998; Chen and Bond, 2010). Mineral matter and some organic compounds mainly from biomass burning (BB) emissions, called brown carbon (BrC), can also absorb solar radiation in the UV range of the solar spectrum. BrC contains a large and variable group of organic compounds including humic substances, polyaromatics hydrocarbons and lignin (Andreae and Gelencsér, 2006), and it is formed by inefficient combustion of hydrocarbons (biomass burning) and also by photo-oxidation of biogenic particles (Yang et al., 2009). The light absorption by mineral dust depends on its content of ferric oxides (Sokolik and Toon, 1999; Alfaro et al., 2004).

Thus, the study of the relationship between physicochemical and optical properties of aerosols is strongly required in order to obtain a deeper characterization of atmospheric aerosols and, therefore, a better estimation of their radiative forcing. Some parameters can be derived from multi-wavelength scattering and absorption aerosol measurements in order to describe the optical properties as a function of the wavelength. These parameters, such as single scattering albedo (SSA), asymmetry parameter (g), scattering Ångström exponent (SAE), absorption Ångström exponent (AAE) and single scattering albedo Ångström exponent (SSAAE), are determined by the physicochemical properties of aerosols and are called intensive because they do not depend on the particle mass. These intensive properties present a valuable input for climate models, which require accurate information concerning the variability of atmospheric composition for targeted species via comparison with observations (Laj et al., 2009). Given the huge variety of aerosol emission sources and formation and transformation processes, there is a substantial need for accurate real-time aerosol optical measurements to achieve a low-error estimation of the effects that atmospheric particles have on climate coupling experimental measurements and modelling results (IPCC, 2007, 2013).

In order to get a wide coverage of the spatial variability of aerosols, aerosol optical data are obtained all over the world from both in situ and remote measurements. The in situ optical measurements are usually performed in international networks using automatic instruments which provide real-time data at high temporal and spatial resolution. Some of the most relevant networks are Aerosols, Clouds and Trace Gases Research InfraStructure (ACTRIS; www.actris.net), Global Atmospheric Watch (GAW; www.gaw-wdca.org), Aerosol Robotic Network (AERONET; www.aeronet.gsfc.nasa.gov) and NOAA baseline observatory (www.esrl.noaa.gov).

The WMB is affected by a large variety of emission sources: natural sources such as Saharan dust, marine aerosols and wildfire; industrial and urban emissions from densely populated areas along the coastline and transboundary sources from the European continent (Steinbrecher et al., 2009; Rodríguez et al., 2011; Pey et al., 2013a, b; Garcia-Hurtado et al., 2014). The atmospheric dynamics coupled to local orography gives rise to a complex mixture of pollutants (Millán et al., 1997) where aerosol formation and transformation processes take place and the accumulation of pollutants is very frequent (Rodríguez et al., 2002, 2003; Pérez et al., 2004; Jiménez et al., 2006; Pey et al., 2010; Jorba et al., 2013; Pandolfi et al., 2014b). Furthermore, the high occurrence of Saharan dust events (SDEs), especially during the summer period, also contribute strongly to the increment of PM_{10} levels in the WMB (Rodríguez et al., 2001, 2015; Querol et al., 2009; Pey et al., 2013a). In fact, more than 70 % of the exceedances of the PM_{10} daily limit value (2008/50/CE European Directive) at most regional background sites of Spain have been attributed to dust outbreaks (Escudero et al., 2007a). Thus, all these processes lead to a radiative forcing in the WMB that is among the highest in the world (Jacobson, 2001). Nevertheless, there is a large uncertainty in the total radiative forcing by atmospheric aerosols in the Mediterranean area (Mallet et al., 2013). The high occurrence and intensity of SDEs in the WMB give us the opportunity to look deeply into the characterization of the optical properties of mineral dust when mixed with local aerosols. Despite several studies having been published on physical and chemical properties of mineral dust in the WMB region (Rodríguez et al., 2001; Escudero et al., 2007b; Querol et al., 2009; Pey et al., 2013a), very few have studied how SDEs affect the aerosol intensive optical properties (Pandolfi et al., 2011, 2014a; Valenzuela et al., 2015)

Possibly related to the scarce use of biomass burning for domestic heating in the Mediterranean region compared to central and northern Europe, very few studies have been published describing BrC effects on intensive aerosol optical properties in the WMB. However, recent studies have estimated that biomass burning sources in the WMB may contribute more than expected to the measured ambient elemental carbon (EC) and organic carbon (OC) concentrations (Minguillón et al., 2011, 2015; Reche et al., 2012; Mohr et al., 2012; Viana et al., 2013; Pandolfi et al., 2014b). In these studies the biomass burning source was characterized by means of techniques such as positive matrix factorization (PMF) on AMS (aerosol mass spectrometer) or ACSM (Aerosol Chemical Speciation Monitor) data, filter-based analysis of ^{14}C and/or specific chemical tracers such as levoglucosan or K^+. Nevertheless, only few studies have

used multi-wavelength aethalometer data (Sandradewi et al., 2008) in the WMB (Segura et al., 2014).

The main aim of this work is to provide a deep characterization of the intensive optical properties of atmospheric aerosols in the WMB under specific pollution episodes (SDEs and BB). Thus, here we evaluate the feasibility of using the intensive aerosol optical properties for the near-real-time detection of specific atmospheric events in the WMB. A sensitivity study aimed at calibrating the measured intensive aerosol optical properties is presented and discussed. We show that this calibration is needed to take into account the effects of local pollution on the intensive optical properties during SDEs and BB events. Moreover, we provide the range of variability of the calculated intensive optical properties as a function of the intensity of these events. This information is valuable input for models studying the radiative effects of atmospheric aerosols in this very peculiar area. With this aim, we used high-quality data collected at two stations located in the WMB: Montseny (MSY, regional background station; 720 m a.s.l.) and Montsec (MSA, remote station; 1500 m a.s.l.). A list of acronyms used in this work is provided in Table S1 of the Supplement.

2 Methodology

2.1 Sampling sites

Results presented in this study were obtained from data collected at two in situ measurement stations located in the NE Iberian Peninsula (Fig. 1).

The Montseny (MSY) site is a mid-altitude emplacement (720 m a.s.l.), representative of the regional background in the WMB. The MSY measurement station is located in the Montseny Natural Park (41°19′ N, 02°21′ E), 40 km to the NNE of the Barcelona urban area and 25 km from the Mediterranean coast and is frequently affected by anthropogenic emissions (Pérez et al., 2008).

The continental background site Montsec (MSA) is a remote high-altitude emplacement (1570 m a.s.l.) situated on the southern side of the Pre-Pyrenees at the Montsec d'Ares mountain (42°3′ N, 0°44′ E), 140 km to the NW of Barcelona and 140 km to the WNW of Montseny (Ripoll et al., 2014). MSY and MSA sites are integrated into ACTRIS (Aerosol, Clouds and Trace gases Research Infrastructure) and GAW (Global Atmosphere Watch) networks, and then in situ aerosol optical measurements were performed following the standards required by these networks.

Detailed information on these monitoring stations can be found, for example, in Pérez et al. (2008), Pey et al. (2009), Pandolfi et al. (2011), Cusack et al. (2012) and Minguillón et al. (2015) for MSY, and in Ripoll et al. (2014, 2015), Pandolfi et al. (2014a) for the MSA site.

2.2 Classification of atmospheric scenarios

The classification of atmospheric episodes affecting the MSA and MSY sites on each day of the sampling period was performed following the procedure described by Ripoll et al. (2014) using BSC-DREAM8b (Basart et al., 2012), SKIRON (Nickovic et al., 2001) and HYSPLIT (Draxler and Rolph, 2015; Rolph, 2015) models.

A detailed description of the main meteorological processes affecting the area under study can be found in Pérez et al. (2008), Pey et al. (2010), Pandolfi et al. (2014a), Ripoll et al. (2014). This study is focused on the atmospheric scenarios which significantly affect the concentrations of pollutants in the WMB: northern African (NAF), summer regional (REG) and Atlantic advection (AA). SDEs, driven by NAF air masses, are more frequent from March to October, strongly contributing to increased PM_{10}. The summer REG scenarios favour the dispersion of the pollutants around the emission sources and the transport and accumulation of pollutants through the regional recirculation of air masses (Millán et al., 1997). Often REGs occur after SDEs, causing important effects on air quality as shown later. AAs affect the WMB throughout the year but mainly in winter. Fresh and clean air masses from the Atlantic clear out the previously accumulated stagnated air masses, leading to lower pollutant concentrations at regional scale. The seasonal distribution of the main atmospheric episodes throughout the year is very similar at MSY and MSA. However, during colder periods MSA high-altitude station is frequently within the free troposphere conditions whereas the MSY station is frequently affected by regional/local emission sources being often within the planetary boundary layer PBL (Pandolfi et al., 2014a, b).

The African dust contribution to PM_{10} (%dust) at MSY was calculated using the statistical methodology described in Escudero et al. (2007b) and Pey et al. (2013). This method is based on the application of a 30-day moving 40th percentile to the daily PM_{10} data series, after excluding those days impacted by African dust. For those days affected by African dust, the percentile value is assumed to be the theoretical background concentration of PM if African dust did not occur. After that, the African dust daily contribution is obtained as the difference between the experimental PM_{10} concentration and the calculated 40th percentile value.

2.3 Measurements and instrumentation

2.3.1 Aerosol absorption and equivalent black carbon (BC) concentration measurements

Aerosol light absorption coefficient (σ_{ap}) at 637 nm (Müller et al., 2011a) was measured at 1 min resolution with a Multi-Angle Absorption Photometer (MAAP, model 5012, Thermo). BC mass concentrations (Petzold et al., 2013) were calculated assuming a constant mass absorption cross section (MAC) of 6.6 $m^2\,g^{-1}$ (Petzold and Schönlinner, 2004).

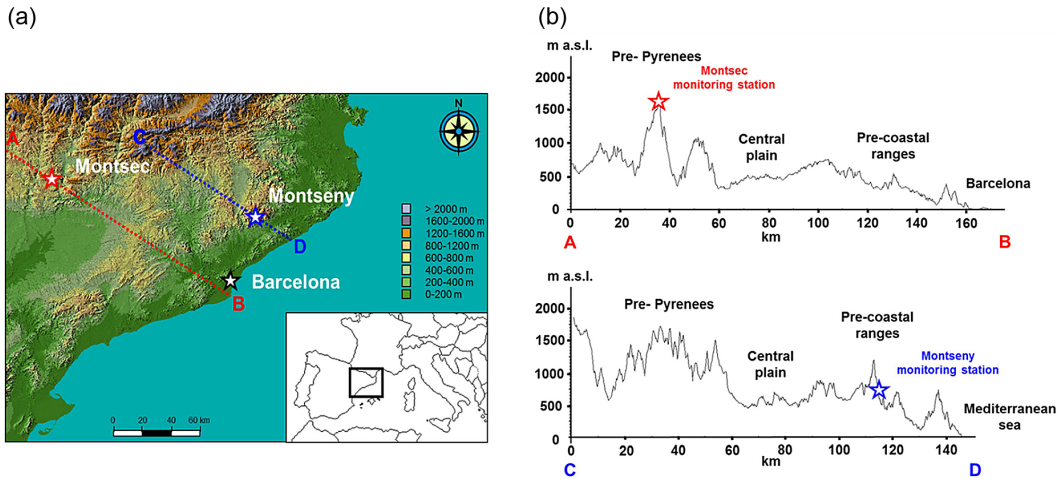

Figure 1. **(a)** Location of Montsec (MSA; remote mountain-top) and Montseny (MSY, regional background) measurement sites. **(b)** Topographic profile of MSA and MSY area.

The detection limit of the MAAP instrument is lower than 100 ng m^{-3} over 2 min integration.

Aerosol light absorption coefficients (σ_{ap}) at seven different wavelengths (370, 470, 520, 590, 660, 880 and 950 nm) were obtained every 1 min at both stations by means of aethalometer instruments (models AE-31 and AE-33). At the MSA site the AE-33 (Drinovec et al., 2015) was equipped with a $PM_{2.5}$ cut-off inlet until March 2014 and with a PM_{10} cut-off inlet afterwards. Absorption measurements at MSY were carried out with a PM_{10} cut-off inlet using an AE-31 aethalometer model from June 2012 to June 2013, then replaced with an AE-33 model. Absorption measurements from the AE-31 were corrected for loading and scattering effects according to Weingartner et al. (2003). The site-specific AE-31 multiple-scattering correction factor (C) at MSY was obtained by comparing simultaneous AE-31 and MAAP measurements. Data was normalized to standard conditions (273 K, 1013 hPa). Multi-wavelength aerosol absorption measurements used in this work cover a period of 2.5 years at MSY (June 2012–December 2014) and around 1 year at MSA (November 2013–December 2014).

2.3.2 Aerosol scattering measurements

Aerosols light scattering (σ_{sp}) and hemispheric backscattering (σ_{bsp}) coefficients were measured at each site every 5 min at three different wavelengths (450, 525 and 635 nm) with a LED-based integrating nephelometer (model Aurora 3000, ECOTECH Pty, Ltd, Knoxfield, Australia). Calibration of the nephelometer was performed 3 times per year by using CO_2 as span gas while zero adjustments were performed once per day by using internally filtered particle-free air. A relative humidity (RH) threshold was set following the ACTRIS recommendations (RH < 40 %). Scattering measurements were corrected for truncation due to non-ideal detection of scattered radiation following the procedure described in Müller et al. (2011b). Multi-wavelength aerosol scattering measurements used in this work cover a period of 5 years at MSY (from January 2010 to December 2014) and 3.5 years at MSA (from July 2011 to December 2014).

2.3.3 PM measurements

Real-time PM concentrations were continuously measured at 30 and 5 min resolution by optical particle counters (OPC) using GRIMM spectrometers (GRIMM 180 at MSY and GRIMM 1107 and GRIMM 1129 at MSA). Concentrations were corrected by comparison with 24 h gravimetric mass measurements of PM_x (Alastuey et al., 2011). For gravimetric measurements, 24 h PM_x samples were collected every 4 days on 150 mm quartz micro-fiber filters (Pallflex QAT) with high-volume (Hi-Vol) samplers (DIGITEL DH80 and/or MCV CAV-A/MSb at 30 m^3 h^{-1}).

3 Calculation of the intensive aerosol optical properties

The extensive and intensive aerosol optical properties and the equations used to derive the intensive properties are reported in Table 1 and briefly commented on below.

In order to study some of the aforementioned intensive optical properties over a wider spectral range, the 3λ scattering measurements from the nephelometer were derived at 7 aethalometer wavelengths using the SAE calculated from 3λ measured scattering. Once scattering was obtained at 7λ, we estimated SSA and SSAAE at these 7λ.

a. The SAE depends on the physical properties of aerosols and mainly on the size of the particles. Generally, SAE lower than 1 or higher than 2 indicates that the scattering is dominated by larger or finer particles respectively

Table 1. Extensive and intensive aerosol optical properties measured and derived respectively in this work.

Extensive optical properties				
Optical properties of PM_{10} particles	Symbol	λ [nm]	Method	Notes
Scattering	$\sigma^{\lambda}_{spPM_{10}}$	450, 525, 635	Nephelometer [AURORA 3000 ECOTECH Pty, Ltd, Knoxfield, Australia]	Measurements corrected for truncation and non-Lambertian illumination function of the light source as in Müller et al. (2011b)
Backscattering	$\sigma^{\lambda}_{bspPM_{10}}$			
Absorption	$\sigma^{\lambda}_{apPM_{10}}$	370, 470, 520, 590, 660, 880, 950	Aethalometer model AE-31 and AE-33[MAGEE Scientific]	AE-31 measurements corrected for filter loading as in Weingartner et al. (2003) and Collaud Coen et al. (2010)
Intensive optical properties				
Scattering Ångström exponent	SAE	450 to 635	$\mathrm{SAE} = -\mathrm{Linear\ estimation}\left(\frac{\mathrm{Ln}\left(\sigma^{\lambda_1}_{spPM_{10}}\ \mathrm{to}\ \sigma^{\lambda_3}_{spPM_{10}}\right)}{\mathrm{Ln}(\lambda_1\ \mathrm{to}\ \lambda_3)}\right)$	
Absorption Ångström exponent	AAE	370 to 950	$\mathrm{AAE} = -\mathrm{Linear\ estimation}\left(\frac{\mathrm{Ln}\left(\sigma^{\lambda_1}_{apPM_{10}}\ \mathrm{to}\ \sigma^{\lambda_7}_{apPM_{10}}\right)}{\mathrm{Ln}(\lambda_1\ \mathrm{to}\ \lambda_7)}\right)$	
Asymmetry parameter	g	450, 525, 635	$g(\lambda) = -7.14\left(\sigma^{\lambda}_{bsp}/\sigma^{\lambda}_{sp}\right)^3 + 7.46\left(\sigma^{\lambda}_{bsp}/\sigma^{\lambda}_{sp}\right)^2 - 3.96\left(\sigma^{\lambda}_{bsp}/\sigma^{\lambda}_{sp}\right) + 0.9893$	The nephelometer measures hemispheric backscattering [−90 to +90°]
Single scattering albedo	SSA	370, 470, 520, 590, 660, 880, 950	$\mathrm{SSA}(\lambda) = \frac{\sigma^{\lambda}_{sp}}{\sigma^{\lambda}_{sp}+\sigma^{\lambda}_{ap}}$	In order to estimate SSA at 7λ, the scattering was calculated at 7λ using the measured SAE.
Single scattering albedo Ångström exponent	SSAAE	370 to 950	$\mathrm{SSAAE} = -\mathrm{Linear\ estimation}\left(\frac{\mathrm{Ln}\left(\mathrm{SSA}^{\lambda_1}_{PM_{10}}\ \mathrm{to}\ \mathrm{SSA}^{\lambda_7}_{PM_{10}}\right)}{\mathrm{Ln}(\lambda_1\ \mathrm{to}\ \lambda_7)}\right)$	

(Seinfeld and Pandis, 1998; Schuster et al., 2006). In this study, SAE was estimated from a linear fit of 3λ scattering measured in the 450–635 nm range.

b. The g parameter (Delene and Ogren, 2002; Andrews et al., 2006) is defined as the cosine-weighted average of the phase function, which is the probability of radiation being scattered in a given direction. Values of g can range from −1 for 180° backward scattering to +1 for complete forward scattering (0°). A value of 0.7 is commonly used in radiative transfer models (Ogren et al., 2006).

c. The AAE provides information about the chemical composition of atmospheric aerosols. BC absorbs radiation across the whole solar spectrum with the same efficiency, thus it is characterized by AAE values around 1 (Kirchstetter et al., 2004; Kim et al., 2012). Conversely, BrC and mineral dust show strong light absorption in the blue to ultraviolet spectrum leading to AAE values up to 3 and 6.5 respectively (Kirchstetter et al., 2004; Chen and Bond, 2010; Kim et al., 2012; Petzold et al., 2009). AAE was estimated from a linear fit of 7λ absorption measured in the 370–950 nm range.

d. The SSA parameter is defined as the ratio between the scattering and the extinction coefficients at a given wavelength and describes the relative importance of scattering and absorption on radiation. Thus, the SSA parameter indicates the potential of aerosols for cooling or warming the atmosphere. A detailed description of SSA at both MSY and MSA was presented by Pandolfi et al. (2011, 2014a). Nevertheless, in this work the SSA is used with the main objective of calculating SSAAE.

e. The wavelength dependence of the SSA is known as the SSAAE and it is defined as SSAAE = (1-SSA) × (SAE-AAE) (Moosmüller and Chakrabarty, 2011). This parameter provides general information about the type of sampled aerosols integrating both physical and chemical properties, and it has been proposed as a good indicator for the presence of Saharan dust in the atmosphere (Collaud Coen et al., 2004). The Saharan dust outbreaks change the intensive optical properties of sampled aerosols, causing a reduction of SAE and an increase of AAE, resulting in a negative SSAAE during these events. Therefore, this parameter can be used to assess which type of aerosol is dominating the scattering and the absorption. For example Collaud Coen et al. (2004) reported measurements performed at the high-altitude alpine station Jungfraujoch (Switzerland) and showed that the SSAAE was able to detect 100 % of Saharan dust outbreaks compared with 80 % and around 40 % of events detected using SAE and AAE respectively. Russell et al. (2010) has also performed the AAE and SSAAE parameters for full aerosol vertical columns obtained from sun-sky photometer retrievals, in order to characterize aerosol columns dominated by the two important sources of UV absorbing aerosols, biomass burning and Saharan dust. The SSAAE was estimated from a linear fit of 7λ-SSA calculated in the 370–950 nm range (Table 1).

4 The aethalometer model

The aethalometer (AE) model allows the detection of fossil fuel combustion (FF) and biomass burning (BB) contributions to the total BC concentrations taking advantage of the different spectral absorption efficiency of the main markers of these two sources: BC for FF combustion and BrC for BB (Sandradewi et al., 2008b). The AE model has also been applied for FF and BB source apportionment to total carbonaceous material ($CM_{total} = OM + BC$) and to organic matter (OM) (Favez et al., 2010). Light absorption measurements at 370–450 and 880–950 nm are used due to the fact that BC from FF combustion has a weak dependence on wavelength whereas BrC from BB shows enhanced absorption at shorter wavelengths. Here we applied the AE model to absorption measurements performed at 370 and 950 nm.

The AE model is usually applied selecting AAE values around 0.8–1.1 for BC from FF combustion (AAE_{ff}) and around 1.6–2.2 for BB (AAE_{bb}). It is known that the AE method may lead to high uncertainties in the estimation of biomass burning contribution due to the high variability of AAE_{bb} depending on the wood-burned combustion regime and on the internal mixing with non-absorbing materials (Lewis et al., 2008; Harrison et al., 2013). Thus, AAE_{ff} and AAE_{bb} are usually chosen by comparing the AE model outputs with FF and BB contributions to BC and/or OM from other techniques such as chemical mass balance (CMB) model on offline filter measurements, positive matrix factorization (PMF) model on AMS and/or ACSM data or ^{14}C technique (Favez et al., 2010; Herich et al., 2011; Crippa et al., 2013). Here we followed a similar procedure to calibrate the AE model: the optimal AAE_{ff} and AAE_{bb} were selected, comparing results from the AE model with those obtained from PMF on simultaneous ACSM hourly data at the MSY station for 1 year (Minguillón et al., 2015). Then, the optimal AAE_{ff} and AAE_{bb} for MSY were applied to MSA aethalometer model.

In the present work, CM_{total} was calculated as the sum of BC concentration measured by MAAP (637 nm) and OM measured by ACSM. Following Eqs. (1)–(3), CM_{total} was expressed as the sum of carbonaceous material from FF combustion (CM_{ff}), carbonaceous material from BB emissions (CM_{bb}) and non-combustion organic aerosols (OA). At the MSY station, OA may account for a large contribution mainly in summer and includes principally organic aerosols from biogenic origin as reported in Minguillón et al. (2011) and Pandolfi et al. (2014b). Thus, we included the constant C_3 in contrast to previous studies, where it was negligible assuming a low contribution of OA sources. CM_{ff} and CM_{bb} were then expressed as the product of the constants (C_1 and C_2) multiplied by the aerosol absorption due to FF at 950 nm ($b_{abs,ff,950}$) and the aerosol absorption due to BB at 370 nm ($b_{abs,bb,370}$) respectively. The $b_{abs,ff,950}$ and $b_{abs,bb,370}$ were calculated for different values of AAE_{ff} and AAE_{bb} following the equations reported in Sandradewi et al. (2008) and then used in Eqs. (1)–(3) for OM source apportionment. Finally, the constants C_1, C_2 and C_3, which related the light absorption to the particulate mass, were calculated using multilinear regression (MLR) analysis.

$$CM_{total} = CM_{ff} + CM_{bb} + OA \quad (1)$$

$$OM + BC = C_1 b_{abs,ff,950} + C_2 b_{abs,bb,370} + C_3 \quad (2)$$

$$OM + BC = (OM_{ff} + BC_{ff})_{950} + (OM_{bb} + BC_{bb})_{370} + OA \quad (3)$$

Once BC_{ff}, BC_{bb}, CM_{ff} and CM_{bb} have been estimated, the contributions of FF and BB to OM (OM_{ff} and OM_{bb}) can be calculated by subtracting BC from CM (Favez et al., 2010).

5 Results and discussion

5.1 General features

Mean, standard deviation, median, minimum, maximum, skewness and percentiles (5, 25, 50, 75, 95) of hourly extensive and intensive aerosol optical properties used in this work are reported in Table S2 for MSY and MSA. Although the periods considered at the two stations were different, time coverage was sufficiently large to allow for a characterization of the mean aerosol optical properties at the two sites.

Mean values of scattering, backscattering and PM_{10} concentrations at both sites were consistent with previous studies performed at these stations (Pandolfi et al., 2011, 2014a; Ripoll et al., 2014, 2015). Higher σ_{sp} and σ_{bsp} were on average measured at MSY consistent with higher PM_{10} concentrations due to the larger impact of anthropogenic sources at this station. Consequently, larger absorption σ_{ap} (Mm^{-1}) at 470 and 880 nm was also observed at MSY (7.66 ± 6.5 and 3.51 ± 2.99) than at MSA (3.57 ± 3.95 and 1.59 ± 1.71).

Mean values of g (525 nm), SAE and AAE at MSY were 0.59 ± 0.06; 1.38 ± 0.79 and 1.30 ± 0.30 respectively. At MSA, mean values for these parameters were 0.57 ± 0.14, 1.58 ± 0.83 and 1.36 ± 0.27. Mean SAE was higher at the MSA station compared to MSY, which could be explained by a dominance of smaller particles on average at MSA, likely due to the frequent position of the station within the free troposphere in winter. As already reported (Andrews et al., 2011; Berkowitz et al., 2011; Marcq et al., 2010; Pandolfi et al., 2014a), under low aerosol loadings at mountain-top sites, in which large aerosols scattering particles have been preferentially removed, the aerosol mixture is mainly composed of relatively smaller and darker particles. Previous studies at MSA have described the free troposphere conditions, characterized by very low PM_1 concentrations ($< 1.5\,\mu g\,m^{-3}$), low values of SSA (0.83) and g (0.43) parameter and increasing SAE (Pandolfi et al., 2014a). The MSY site presented slightly lower AAE values compared to MSA, due to a major predominance of black carbon particles as a consequence of the proximity to the Barcelona urban area. SSA was slightly higher at MSA (0.85 ± 0.08 and 0.82 ± 0.3) than MSY values (0.83 ± 0.07 and 0.8 ± 0.12) at 470 and 880 nm respectively.

5.2 Detection of Saharan dust outbreaks using aerosol intensive optical properties

As already observed, SDEs can be detected using measurements of optical properties, taking advantage of the changes that mineral dust causes in the spectral dependence of aerosol scattering and absorption (Collaud Coen et al., 2004). In fact, SDE scenarios are characterized by a decrease of SAE, as a consequence of the predominance of coarse particles, and an increase of AAE due to the enhanced absorption in the UV spectrum by mineral dust. The angstrom matrix is a useful tool for detecting periods dominated by SDEs (Russell et al., 2010). It consists of a scatter plot made up of the SAE parameter on the x axis and the AAE parameter on the y axis, providing information about aerosol size and composition. The scatter plot can be colour coded and investigated by other parameters to further characterize the atmospheric aerosols. In our case the matrix was colour coded for different air mass origins and by the coarse fraction contained within the PM_{10} ($\%PM_{1-10}$ in PM_{10}), which was calculated as the difference between $\%PM_1$ and $\%PM_{10}$ contained within the PM_{10} fraction.

The Ångström matrix for MSY and MSA (Fig. 2b, e) showed dominance of coarse material (high % of PM_{1-10} in PM_{10}) related to low values of SAE (roughly lower than 1) and larger values of AAE (approximately higher than 1.3) during SDEs.

In order to demonstrate that these SAE and AAE limits were mainly related with the presence of mineral dust from Africa in the area under study, the Ångström matrices were also investigated by the occurrence of the three main atmospheric situations affecting MSY and MSA stations: SDEs, REGs and AAs (Fig. 2a, d). As shown in Fig. 2a, d, the region of the Ångström matrices representing SDEs fits well with the SAE and AAE limits reported above (Fig. 2b, e). Averages and standard deviations of SAE and AAE during SDEs were 1.12 ± 0.87 and 1.27 ± 0.24 for MSY, and 0.69 ± 0.78 and 1.41 ± 0.25 for MSA. Lower SAE and higher AAE at MSA pointed to a larger dominance of mineral dust and a purer composition during these events at the high-altitude station (Fig. S1). Average PM_{10} concentrations during SDEs were 25.4 ± 17 and $21.0 \pm 17\,\mu g\,m^{-3}$ for MSY and MSA respectively. Further information providing the frequency distribution and average values of SAE, AAE, PM_{10} and $\%PM_{1-10}$ in PM_{10} for each atmospheric situation at both stations is reported in Fig. S1 of the Supplement.

The feasibility of detecting Saharan dust outbreaks by means of the hourly Ångström matrices is further confirmed in Fig. S2, where the Ångström matrix for the MSY station was weighted by the %dust (daily basis) for those days affected by SDEs. The quantification of African mineral dust contribution to PM_{10} (%dust) at MSY was calculated using the statistical methodology described in Escudero et al. (2007b) and Pey et al. (2013a) (detailed in Sect. 2.2). Despite the scarce availability of simultaneous daily data points of SAE, AAE and %dust for the period under study, the Ångström matrix showed lower SAE and increasing AAE with increasing intensity of SDEs (% dust) in agreement with the Ångström matrix reported in Fig. 2b. However, Fig. S2 clearly shows that there are conditions when the AAE-SAE pair does not unequivocally detect the Saharan dust outbreaks, being SAE higher than 1.0–1.5 and AAE lower than 1.2–1.3. These points are characterized by relatively low (< 40 % approximately) dust contribution to PM_{10} representing not very intense SDEs. Thus, this region of the Ångström matrix identified an aerosol mixture between mineral dust and anthropogenic pollutants of mainly local origin. Then, we can conclude that (a) some points during REG episodes (yellow dots in Fig. 2a, d) were characterized by SAE and AAE values similar to those observed during SDEs, indicating presence of mineral dust in the atmosphere and (b) for some SDEs, the corresponding AAE-SAE pairs do not unequivocally confirm the presence of mineral dust (anthropogenic emissions and mineral dust mixing).

The blue spot area displayed in the Ångström matrix for the MSA station (Fig. 2e) showed AAE-SAE pairs characterized by low contribution of PM_{1-10} to $PM_{10} \sim$ %1–10,

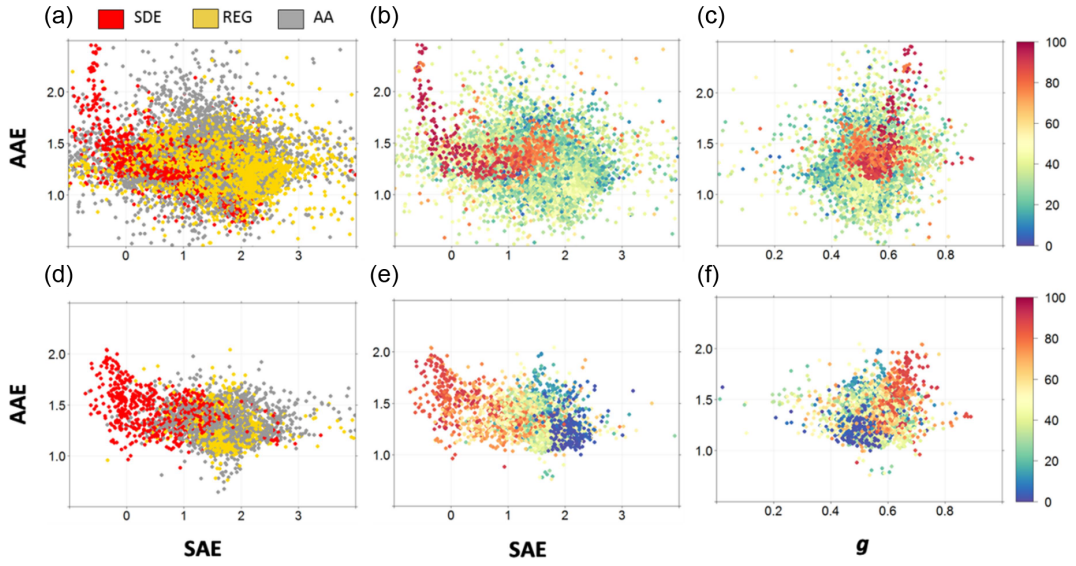

Figure 2. Ångström matrix (scatter plot of AAE vs. SAE weighted by air mass origin) at **(a)** MSY and **(d)** MSA. Ångström matrix (scatter plot of AAE vs. SAE weighted by levels of $\%PM_{1-10}$ in PM_{10}) at **(b)** MSY and **(e)** MSA. Ångström-asymmetry parameter matrix (scatter plot of AAE vs. g weighted by levels of $\%PM_{1-10}$ in PM_{10}) at **(c)** MSY and **(f)** MSA (on an hourly basis).

which are mainly represented by AA scenarios. Average and standard deviation of SAE and AAE during these scenarios were 1.35 ± 0.95 and 1.33 ± 0.27 for MSY, and 1.65 ± 0.57 and 1.30 ± 0.16 for MSA respectively. PM_{10} showed the lowest concentrations during these events, being 11 ± 7 and $9.4 \pm 6\,\mu g\,m^{-3}$ respectively for MSY and MSA (Fig. S1). These AA scenarios, some of them related with free troposphere conditions in MSA during winter, lead to a cleaner environment, free of pollutants and characterized by finer and relatively darker particles in the Ångström matrix. Conversely, a predominance of REG scenarios is seen at MSY (yellow dots in Fig. 2a), related to larger contribution of PM_{1-10} to PM_{10} (40–80 %) (Fig. 2b). SAE and AAE values during REG episodes were 1.61 ± 0.87 and 1.24 ± 0.19 for MSY and 1.66 ± 0.48 and 1.29 ± 0.15 for MSA. The average PM_{10} concentrations during these atmospheric situations were 15.6 ± 8 and $12.6 \pm 7\,\mu g\,m^{-3}$ for MSY and MSA (Fig. S1). REG episodes, mainly related to pollution scenarios, are characterized by local (affecting lower-altitude regions driven by the breeze patterns) to regional (reaching higher-altitude locations driven by larger circulations and upslope winds) atmospheric circulations transporting fine particles from the urbanized/industrialized coastline. SAE ranged between 0–3 and 1–2.5 at MSY and MSA stations respectively during REG scenarios, whereas main AAE values ranged between 1–1.7 at both stations. Recently, Mallet et al. (2013) reported column-integrated AAE (440–870 nm) values across the Mediterranean using Level 2 AERONET data varying from around 1.3 in urban areas to more than 2 at Mediterranean dusty sites.

In order to study how SDEs affect the asymmetry parameter in the area under study, Fig. 2c and f show a modified Ångström matrix where the g parameter was investigated instead of SAE at both stations. This parameter can also be used to estimate the size of aerosols according to the difference in the scattering direction presented by small and larger particles, since larger particles present higher forward scattering than backward scattering. During SDEs, g was similar at both stations, approximately ranging between 0.55 and 0.75 at MSA and between 0.5 and 0.7 at MSY. These results are in agreement with the g values reported by Ogren et al. (2006) for other in situ measurements. Therefore, given that SAE parameter presents larger variability than g in relation to changes in $\%PM_{1-10}$, we conclude that SAE is a better proxy for estimating aerosol size. Despite this, providing experimental variability ranges for g is important given that the asymmetry parameter is commonly used in radiative transfer models (Ogren et al., 2006).

As already mentioned, the SSAAE has been identified as a good indicator for Saharan dust outbreaks at mountain-top sites being negative during these types of events (Collaud Coen et al., 2004). The SSAAE is a useful parameter and can be used together with the Ångström matrix to characterize mineral dust at different emplacements with the aim to identify SDEs in real time. Similarly to what was already observed for the Ångström matrices, our results showed that the feasibility of detecting SDEs by means of SSAAE depended on both the location and altitude of the measurement station, which determines the aerosol background concentration and the intensity of the SDE.

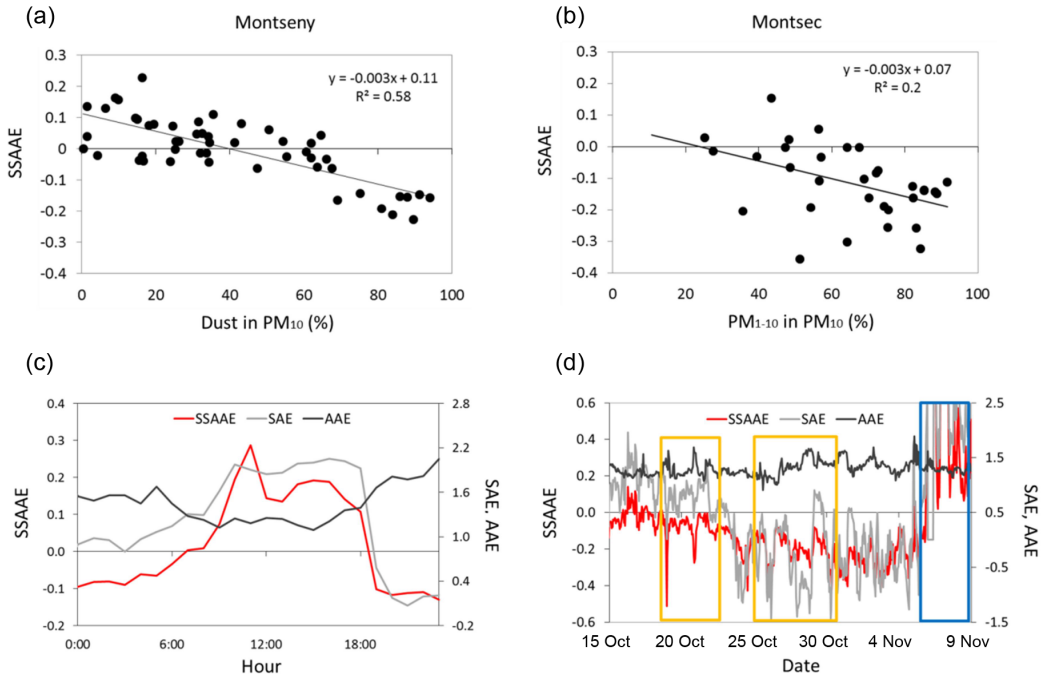

Figure 3. Relationship between SSAAE and the relative contribution (%) of **(a)** mineral dust to PM_{10} at MSY and **(b)** PM_{1-10} to PM_{10} at MSA. Case studies discussed in the text show hourly SAE, AAE and SSAAE calculated for MSY during the periods **(c)** 28 June 2012 and **(d)** 15 October–9 November 2013. Yellow and blue rectangles in Fig. 3d indicate the occurrence of SDEs and precipitation respectively.

Figure 3a showed a relationship between SSAAE and %dust at MSY for those days affected by SDEs. At MSA, where %dust was not calculated due to limitations of the methodology, SSAAE correlated with the percentage of coarse particles in PM_{10} (Fig. 3b). SSAAE became negative for most SDEs identified at MSA, accounting for 85 % detection of these events. However SSAAE showed more frequently positive values near to zero at MSY, detecting 50 % of SDEs due to a larger exposure to anthropogenic emissions. The SSAAE became negative when the relative contribution of Saharan dust to PM_{10} (%dust) at MSY was higher than approximately 60 %, keeping positive values at lower %dust in PM_{10} despite the presence of mineral dust.

Figure 3c shows an example of the daily variation of SSAAE, SAE and AAE at MSY during a SDE. Low values of SAE (< 1) and higher values of AAE (> 1.5) led to negative SSAAE during the night, indicating presence of mineral dust. Conversely, during the day, anthropogenic fine pollutants transported from nearby polluted areas hindered the optical effect of mineral dust during non-intense SDEs (54 % of dust in PM_{10}). Consequently, despite the impact of mineral dust, the SSAAE turned into positive values. SAE reached values around 2, indicating dominance of fine particles and, correspondingly, the AAE lowered to around 1.2, indicative that these fine particles were mainly of anthropogenic origin. Thus, the proximity to anthropogenic sources under specific atmospheric conditions (i.e. strong breeze and low SDE intensity) can prevent both the Ångström matrix and the SSAAE parameter from detecting SDEs.

A different scenario is shown in Fig. 3d, where two Saharan dust outbreaks were detected and highlighted by the yellow rectangles. The SSAAE was negative during the two outbreaks, keeping negative values between the two events despite the influence of Atlantic air masses during the days 23 and 24 October 2013. Interestingly, the SSAAE reached the lowest negative values during the subsequent days after the SDE, until precipitation scavenged pollutants from the atmosphere (highlighted by the blue rectangle). Thus, the local and regional recirculation of air masses under the REG episode, often lasting for a few days, recirculated an aerosol mixture dominated by coarse Saharan particles in the atmosphere at a level able to cause the SSAAE to be negative even in the absence of African air mass advection (Fig. S3). It is interesting to highlight that, despite the intensive optical parameters showing the presence of mineral dust during the REG episode with SSAAE < 0 and the corresponding decreasing SAE and increasing AAE, the BSC-DREAM8b was not able to reproduce the recirculation of mineral dust (Fig. S3d), and only a simulation at high spatial resolution could characterize the event. The evidence that mineral dust can recirculate under dry conditions in summer for a few days after the SDE is of high relevance for air quality. Thus, near-real-time aerosol optical parameters such as SSAAE are very useful for detecting mineral dust in the atmosphere even after the end of the event.

5.3 Detection of biomass burning using aerosol optical properties

5.3.1 Calculation of the constants from the aethalometer model

In order to test the stability of the AE model for our emplacement (MSY), C_1, C_2 and C_3 were calculated, varying (Table 2) (a) AAE_{bb} between 1.8 and 2.2 (for a fixed $AAE_{ff} = 1$) and (b) AAE_{ff} between 0.9 and 1.1 (for a fixed $AAE_{bb} = 2$). In the first case (a) C_1 showed a very low variability keeping values around $1.05 \pm 0.01\,g\,m^{-2}$, whereas C_2 showed a higher variability ranging between $0.28\,g\,m^{-2}$ ($AAE_{bb} = 1.8$) to $0.24\,g\,m^{-2}$ ($AAE_{bb} = 2.2$). In our work, C_3, which represents the contribution from non-combustion OM, was estimated at around $0.31 \pm 0.04\,\mu g\,m^{-3}$. These results were consistent with previous studies dealing with AE source apportionment to OM and reporting less variability for C_1 compared to C_2 (Sandradewi et al., 2008; Favez et al., 2010). In another study (Herich et al., 2011) the AE model was not applied to OM, mainly due to the high variability (i.e. model instability) observed for C_1 from different model outputs. In the second case (b), C_1 changed only a little (less than 10 %), ranging from $1.01\,g\,m^{-2}$ ($AAE_{ff} = 0.9$) to $1.09\,g\,m^{-2}$ ($AAE_{ff} = 1.1$) for a fixed AAE_{bb} of 2. As reported below, AAE_{bb} for our environment was set to 2 by comparison with ancillary experimental measurements, whereas AAE_{ff} was set to 1 as in previous studies, given the lower sensitivity of the AE model to AAE_{ff} compared to AAE_{bb}. It is important to consider that the values of C_1 ($\sim 1.05\,g\,m^{-2}$) and C_2 ($\sim 0.26\,g\,m^{-2}$) calculated for our emplacement were different from those reported in previous studies for different environments. In their works, Favez et al. (2010; Grenoble) and Sandradewi et al. (2008; Roveredo, Switzerland) set C_1 to a fixed value of $0.26\,g\,m^{-2}$, this parameter being less variable, and C_2 was estimated around 0.7–0.8 $g\,m^{-2}$. Differences between the constants were due to the larger use of biofuel for domestic heating in these latter locations, leading to a higher contribution of BB than FF combustion sources to BC (and probably a smaller influence of FF sources). This was contrary to our emplacement where results indicated (as shown later) a higher contribution from FF sources compared to BB for both BC and OM.

Given the large differences between constants obtained in this study (C_1 and C_2) and those previously reported for other environments, here we applied a similar procedure to the one described in Herich et al. (2011). Thus, we simulated CM_{total} using C_1 and C_2 from Sandradewi et al. (2008) and Favez et al. (2010), and $b_{abs,ff,(\lambda 1)}$ and $b_{abs,bb,(\lambda 2)}$ as derived from our measurements. As expected, the results showed a very low correlation between calculated and measured CM ($R^2 = 0.009$; slope = 0.65) compared to $R^2 = 1$ and slope = 1 using our calculated constants C_1, C_2 and C_3. Therefore, we conclude that calculation of the specific constants of the model for the area under study is required to successfully run the aethalometer model.

Moreover, we calculated C_1, C_2 and C_3 for two more cases: (a) we included only the winter season in order to account for a larger contribution of BB emissions and to reduce the influence of non-combustion OM and SOA formation which maximize in summer at the MSY station (Minguillón et al., 2011) and (b) we excluded SDEs from the database which could overlap with BrC being both BB and mineral dust, which are important absorbers in the UV. The differences for C_1, C_2 and C_3 calculated between these two cases and the whole period (June 2012–July 2013, Table 2) in case (a) were lower than 10, 20 and 15 % respectively. These differences were around 3, 6 and 34 % for case (b). Given that the AE model outputs have been estimated with errors as high as 50 % (Favez et al., 2010) and given that we are continuously measuring absorption with the AE instrument at MSY and MSA without ACSM data, the model was calibrated using a 1-year data set in order to apply the AE model to any other period without ancillary measurements.

5.3.2 Validation of the aethalometer model with simultaneous experimental data

Very few studies have been published comparing outputs from the AE model to the source apportionment of the ACSM measurements (Favez et al., 2010). Biomass burning organic aerosol (BBOA) and hydrocarbon-like organic aerosol (HOA) from ACSM data refer to primary organic aerosols (POA), whereas OM_{bb} and OM_{ff} from AE model include SOA formed from these primary sources. Since simultaneous measurements to the study period were not deployed for differentiating POA to SOA ratios, we have considered results previously reported for MSY. SOA formation from biomass burning emissions can be up to 25 % of the BBOA emitted, as shown by Cubison et al. (2011) using aerosol mass spectrometer (HR-ToF-AMS) data. This ratio was primarily applied by Minguillón et al. (2015) to the results obtained from the source apportionment to ACSM performed at the MSY station, which were also used in this study. Moreover, based on the results from the DAURE campaign carried out in March 2009 at MSY, the organic carbon (OC) originated from fossil sources is only 15 % primary at MSY (Minguillón et al., 2011), which corresponds to 10 % if OM is considered instead of OC. Thus, we assume that primary BBOA and HOA represent approximately 75 and 10 % of the OM_{bb} and OM_{ff} respectively at the MSY station.

Relationships between BBOA and OM_{bb} concentration for different AAE_{bb} values (Table 3) showed good agreement ($R^2 \sim 0.43$) with slopes ranging between 1.1 and 2.2 depending on the AAE_{bb} used. The relationship between OM_{ff} and HOA showed less variable slope (F) (around 4) but more variable R^2 between 0.43 and 0.63. Choosing $AAE_{bb} = 2$ and $AAE_{ff} = 1$ we obtained (a) an OM_{bb}/ BBOA ratio of around 1.27 ($R^2 = 0.43$) in agreement with 25 % of SOA for-

Table 2. C_1, C_2 and C_3 obtained by MLR on the aethalometer model for different AAE_{bb} (1.8, 2, 2.2), keeping $AAE_{ff} = 1$ and varying AAE_{ff} (0.9, 1.1), keeping $AAE_{bb} = 2$ on an hourly basis at MSY.

Hourly data (5456)	$AAE_{ff} = 1$		
	$AAE_{bb} = 1.8$	$AAE_{bb} = 2$	AAE_{bb} =2.2
C_1 (g m^{-2})		1.05153 ± 0.01004	
C_2 (g m^{-2})	0.27998 ± 0.00314	0.26021 ± 0.00354	0.24384 ± 0.00393
C_3 (µ g m^{-3})		0.31433 ± 0.04051	
	AAE_{bb} =2		
	$AAE_{ff} = 0.9$	$AAE_{ff} = 1.1$	
C_1 (g m^{-2})	1.01342 ± 0.01063	1.09341 ± 0.00959	
C_2 (g m^{-2})		0.26021 ± 0.00354	
C_3 (µ g m^{-3})		0.31433 ± 0.04051	

Table 3. Squared Pearson (R^2) and slope (F) of the scatter plot between OM_{bb} and BBOA and between OM_{ff} and HOA, for different values of AAE_{bb} (1.6, 1.8, 2, 2.2) keeping $AAE_{ff} = 1$ at MSY (hourly basis).

		$AAE_{ff} = 1$			
	AAE_{bb}	1.6	1.8	2	2.2
OM_{bb} vs. BBOA	R^2	0.436	0.423	0.429	0.426
	F	2.160	1.440	1.274	1.064
OM_{ff} vs. HOA	R^2	0.426	0.525	0.600	0.631
	F	4.002	4.240	4.377	4.467

mation from primary biomass burning emissions estimated by Cubison et al. (2011); and (b) an OM_{ff}/ HOA ratio of 4.4 ($R^2 = 0.6$) which is consistent with 90 % portion of SOA found at MSY in previous studies (Minguillón et al., 2011). The correlations were only moderate mainly due to the variable SOA formation, which is partially driven by the environmental conditions, as opposed to the primary OA emissions. Moreover, it should be noted that the slopes and R^2 in Table 3 were obtained using hourly averages. Scatter plots by bins (Fig. 4) showed that the relationships had slopes in agreement with those reported in Table 3 but much higher R^2 (0.97).

The relationship between OM_{bb} and BBOA calculated only for the winter period using hourly data showed $R^2 = 0.4$ and $F = 0.96$. The slope was close to the unity due: to the lower SOA formation in winter, mainly explained by a decreasing of VOCs emissions being one of the primarily precursor sources of SOA formation during the warmer period in this emplacement (Seco et al., 2013), also as consequence of less photochemistry activity and the prevalence of primary emissions.

Experimental measurements of Nitrogen dioxide (NO_2), which is mainly related to fossil fuel emissions, agrees well ($R^2 = 0.64$) with BC_{ff} obtained from $AAE_{bb} = 2$ and $AAE_{ff} = 1$ for the winter period at MSY (Fig. 5).

Besides uncertainties in determining FF and BB contributions from the aethalometer model, results from sensitivity test analysis showed good agreement with experimental measurements and good stability of the model. We have shown that the constants C_1, C_2 and C_3 depend on the relative contributions of FF and BB, thus these constants are site-dependent and should be calculated for each measurement emplacement. Moreover, a calibration of the model is necessary to determine the most suitable AAE_{ff} and AAE_{bb} pair for a reliable estimation of fossil fuel and biomass burning contributions. Interestingly, AAE_{bb} and AAE_{ff} chosen in this work were the same as in other studies, suggesting a stable value of AAE = 2 for characterizing BB emissions within the model. Our results showed that the higher AAE_{bb} the lower the estimated BC_{bb} contribution, which ranged between 35 and 45 % depending on the AAE_{bb} used (1.8–2.2).

5.3.3 Seasonal and daily variation of fossil fuel and biomass burning contribution to BC and OM at MSY and MSA stations

Seasonal and daily AAE and relative contributions of BB and FF to BC (at both MSY and MSA) and to OM (at MSY only) from the aethalometer model are shown in Fig. 6. Both environments are characterized by similar average PM chemical composition (Ripoll et al., 2015), thus probably leading to similar mean values of AAE at MSY (1.30 ± 0.30) and MSA (1.36 ± 0.26) (Fig. 6a, e). Thus, AAE_{ff} and AAE_{bb} determined for MSY were used also for MSA.

MSY showed slightly lower AAE as a consequence of higher exposure to FF emissions sources compared to MSA. AAE at MSA and MSY showed larger values on average in winter suggesting a higher contribution of BrC. AAE monthly averages reached around 1.5 at both sites. Despite the fact that the lowest BC and OM concentrations were observed in winter the AAE showed the highest values indicat-

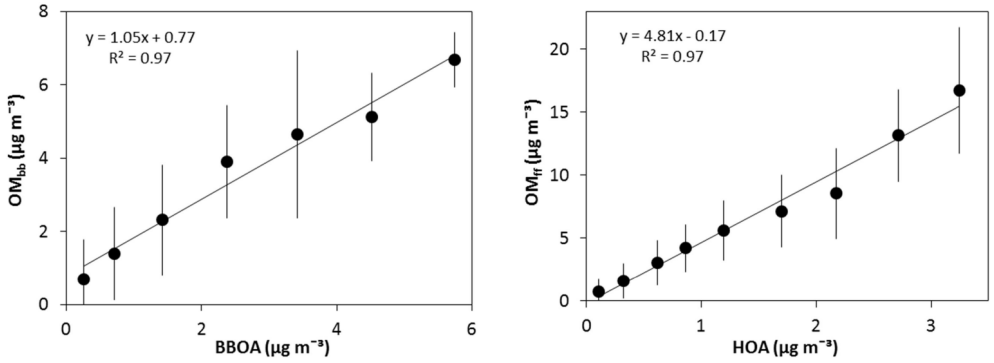

Figure 4. Scatter plot by bins between OM_{ff} and HOA and between OM_{bb} and BBOA for $AAE_{bb} = 2$ and $AAE_{ff} = 1$ at MSY (on an hourly basis).

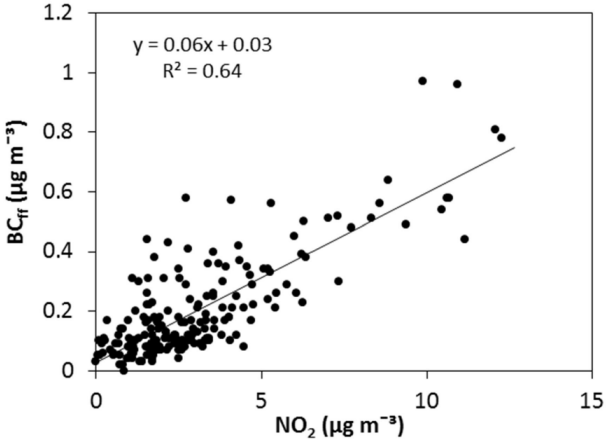

Figure 5. Scatter plot between BC_{ff} and NO_2 for winter season (from November to February,) during the period 2012–2014 at MSY (daily basis).

ing larger contribution of BB sources at both stations. It is interesting to note that on average AAE was higher at MSY than at MSA during winter months (December–January) suggesting higher relative BB contribution at MSY compared to MSA in winter (Figs. 6e and S4a). This was likely due to the fact that the MSA station is often above the polluted PBL in winter whereas MSY, located at lower altitude, is usually within the PBL and frequently affected by local pollutants accumulated under winter anticyclonic conditions (Pandolfi et al., 2014b; Ripoll et al., 2015). Low values of AAE during the day and higher at night at both sites resulted mainly from the development of sea and mountain breezes, favouring the transport of anthropogenic pollutants from the urbanized/industrialized coastline and valleys to inland areas and leading to an increase of AAE during the warmest hours of the day (Fig. 6a).

The measured BC was well reproduced by adding BC_{ff} and BC_{bb} contributions from the AE model, showing slight overestimation by 11 and 15 % at MSY (Fig. 6c, g) and MSA (Fig. 6d, h) respectively. However, measured OM is underestimated when adding OM_{ff} and OM_{bb} at MSY, due to the large contribution of carbonaceous material from non-combustion sources (C_3) during the warmer months (27 %) (Fig. 6f). This difference was mainly driven by biogenic sources which are expected to have an important contribution to our measurement emplacement, particularly in summer due to the SOA formation. Then the C_3 time variation was well reproduced by the model, showing larger contributions during the summer period. Nevertheless, based on the available previous studies performed at MSY (Minguillón et al., 2011, 2015; Pandolfi et al., 2014b), C_3 contribution might be slightly underestimated due to possible apportionment within OM_{ff} and/or OM_{bb}. It should also be noted that some SOA UV absorbing compounds, which originate from anthropogenic sources (such as nitroaromatic compounds) and are the major contributors to the light absorption of the toluene SOA, might be partially apportioned within OM_{bb}.

Interestingly, a relationship was observed between AAE and the relative contribution of BC_{bb} to BC concentrations at MSY and MSA (Fig. 7). AAE increased up to 1.5 when $\%BC_{bb}$ was higher than around 50 % of the total measured BC. The intercept of the linear fit was 1.01 and 1.15 at MSY and MSA respectively, pointing to BC from FF sources as the main absorber in the absence of biomass burning events. Therefore, we can clearly appreciate the effect of BrC from biomass burning on AAE even if the mean BC_{bb} contributions to the total BC (0.13 µg m^{-3} and 0.06 µg m^{-3}) at MSY and MSA were quite low (36 and 40 %). Mean OM_{bb} concentration at MSY was 0.9 µg m^{-3}, accounting for a 30 % contribution to total OM.

The prominent increase of FF contribution at MSY and MSA in summer, when both stations are within the PBL and dominated by similar atmospheric circulations, is in agreement with lower AAE values. Stronger summer recirculation processes, which are strengthened by sea and mountain breezes, favour the transport of pollutants toward regional areas inland. Daily variation of both BC and OM is mainly driven by FF combustion from Barcelona anthro-

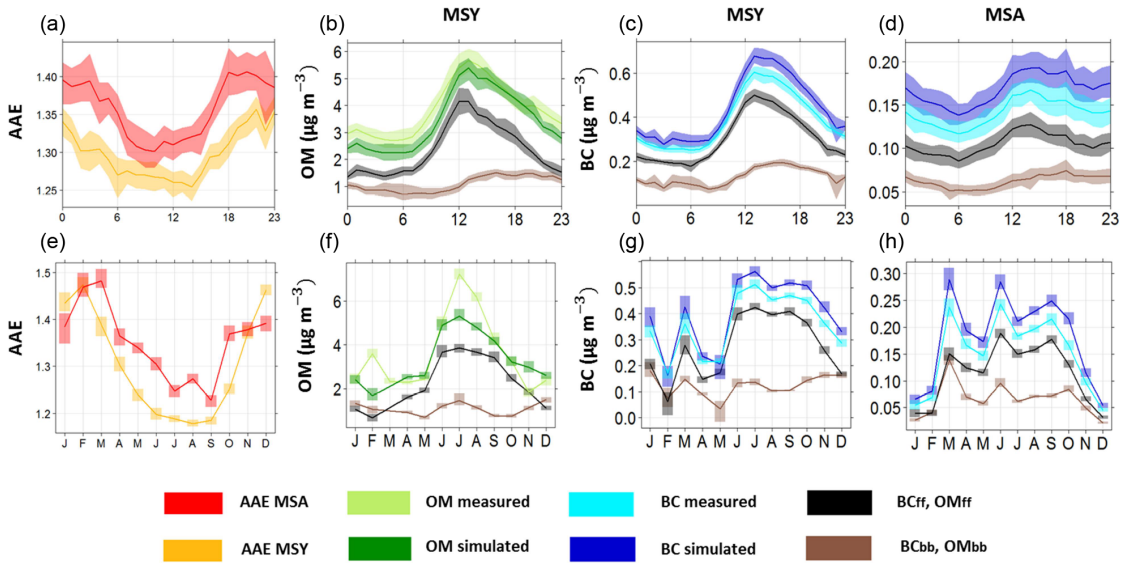

Figure 6. Daily cycle of **(a)** AAE at MSY and MSA, **(b)** measured OM and simulated OM as the sum of OM_{ff} and OM_{bb} contributions at MSY, measured BC and simulated BC as the sum of BC_{ff} and BC_{bb} contributions at **(c)** MSY and **(d)** MSA. Annual cycle of **(e)** AAE at MSY and MSA, **(f)** measured OM and simulated OM as the sum of OM_{ff} and OM_{bb} contributions at MSY, measured BC and simulated BC as the sum of BC_{ff} and BC_{bb} contributions at **(g)** MSY and **(h)** MSA. The study period ranges between 14 June 2012 and 9 July 2013 for OM contributions and between 12 June 2012 and 31 December 2014 for BC contributions, depending on the availability of BC and OM experimental measurements respectively. Averages were calculated on an hourly basis.

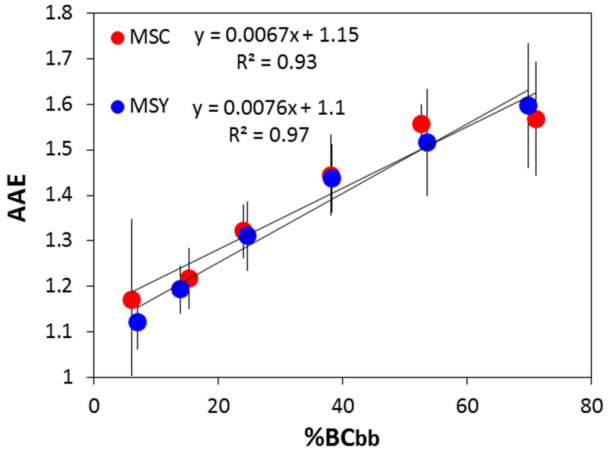

Figure 7. Scatter plot by bins between AAE and $\%BC_{bb}$ at MSY and MSA. Error bars are one standard deviation of the averages calculated from daily values.

pogenic sources. The daily cycle is more pronounced at MSY as a consequence of the proximity to the Barcelona metropolitan area and the lower altitude compared to MSA. Despite OM is mainly driven by biogenic sources during the summer period at MSY, significant FF contribution is registered during the warmest hours of the day (Fig. S4b). However time variation of BB sources, from both BC and OM, is led by local atmospheric processes as domestic heating turning into a dominant source during the colder months at both stations. Thus, during winter, BC_{bb} and BC_{ff} showed almost the same contribution, reaching maximum values in the afternoon (Fig. S4c). Conversely, the daily cycle of OM_{ff} is decoupled from OM_{bb}, showing larger concentrations of the latter during the night, given that it is mainly led by BB emissions from domestic heating emitted during the colder hours and possibly as a result of SOA formation after the OM was emitted (Fig. S4b). Note that during the night OM_{bb} concentration does not present large variations, possibly because it remains as a residual layer above the thermal inversion.

FF contribution to OM and BC was found to be significant at MSY, according to the large values obtained for the C_1 constant in the aethalometer model. In order to compare the results with different source apportionment methods, the fossil fuel and non-fossil fuel contribution to EC (EC_{ff}, EC_{non_ff}) and OC (OC_{ff}, OC_{non_ff}) reported by Minguillón et al. (2011) using the ^{14}C technique at MSY for the periods February–March and July 2009 were taken as a reference. Given that AE measurements were not available at MSY during those periods, we averaged available contributions from the aethalometer model for the same time-of-the-year periods during 2012, 2013 and 2014 for BC and during 2012 for OM. Despite the lack of overlap in the data set, results for BC contributions from both techniques (^{14}C and AE model) showed good agreement. BC_{ff} contributions calculated using the AE model in winter and summer were 53 and 73 % respectively, whereas EC_{ff} contributions derived from ^{14}C measurements accounted for 66 and 79 %. However larger discrepancies were found for FF and BB contributions to OM. Results from

the ^{14}C technique identified a FF contribution to OC of 31 and 25 % for winter and summer, whereas the AE model resulted in OM_{ff} contributions of 39 and 58 %. We also saw a OM_{bb} contribution around twice that of the OC non-fossil fuel. The apparent overestimation of OM_{bb} and OM_{ff}, particularly in summer, compared to the available results from ^{14}C might be led by the partial apportionment of non-combustion carbonaceous material and SOA anthropogenic within OM_{bb} and/or OM_{ff}, as we commented above.

A second assessment of the AE model results was carried out by comparison with OA source apportionment results reported by Minguillón et al. (2015) for winter (28 October–7 April 2013) and summer (14 June–9 October 2012) at MSY based on ACSM measurements. The agreement needs to be evaluated considering the different outputs from each method; thus whereas the ACSM OA source apportionment identifies the contribution of primary fossil fuel (HOA) and biomass burning (BBOA) contributions, the AE model calculates the total (including the SOA) fossil fuel (OM_{ff}) and biomass burning (OM_{bb}) contributions. HOA contribution was 12 and 13 % for winter and summer, whereas OM_{ff} accounted for 47 and 59 %. BBOA was identified only in winter with a contribution of 28 %, and OM_{bb} contribution was 37 % for the same period. These results are in agreement assuming the ratios OM_{ff}-to-HOA and OM_{bb}-to-BBOA based on SOA-to-POA proportion, used in the previous Sect. 5.4.3 in order to calibrate the aethalometer model and fit the most suitable AAE_{ff} and AAE_{bb} representative of our environment.

An interesting wildfire episode detected at MSY took place on 23 July 2012 with AAE increasing significantly up to 2 and the lowest value at 1.3 (Fig. 8). BB sources dominated BC and OM contributions accounting for 73 % and 78 % respectively, until the breezes were developed and transported pollutants from urban areas toward the station during the warmest hours of the day, resulting in a decrease of AAE. As shown previously for the whole data set, good agreement was found between measured and simulated BC. Conversely OM was slightly underestimated during the sunlight hours likely due to biogenic emissions and SOA formation by photochemical reactions.

The concomitance of biomass burning and wildfire episodes during SDEs may be an issue, being both dust and BB strong absorbers in the UV. The SAE is a useful parameter that should be considered in order to establish differences in near real time between mineral dust (coarse material) and biomass burning (finer aerosol). However, since relatively low BB concentration was found in the area under study, the dominance of mineral dust appears to be larger with respect to BB regarding the effects on intensive optical properties. Furthermore, the co-occurrence of SDEs and BB winter emissions is not usual. Whereas for differentiating wildfires episodes and SDEs, both frequently occurring during summer, wildfires can be considered isolated events and detected by different tools such as back-trajectories, forecast models and remote sensing data.

6 Conclusions

The present work shows variations of the intensive aerosol optical properties measured at regional (Montseny) and continental (Montsec) background stations in the WMB. We have studied the feasibility of using the near-real-time optical measurements performed at these stations for the detection of specific atmospheric pollution episodes affecting the WMB: Saharan dust and biomass burning.

The Ångström matrix revealed that Saharan dust events (SDEs) in the WMB were characterized by SAE on average lower than 1 due to the larger size of mineral dust particles and AAE values higher than 1.3 (up to 2.5 depending on the intensity of SDEs), indicating absorption in the UV by iron oxide contained within the mineral dust. Linear relationships were found between AAE and increasing %dust at MSY (0.7) and $\%PM_{1-10}$ at MSA (0.4), confirming the enhanced absorption in the UV due to mineral dust from SDEs. Interestingly, SAE showed higher sensitivity than g for characterizing the size of aerosols, with ranges between 0.55–0.75 and 0.50–0.70 at MSY and MSA respectively during SDEs.

Feasibility of detecting SDEs by means of SSAAE depended on both the location and altitude of the measurement station, which determines the aerosol background concentration and the intensity of the SDE. Better results were shown at higher-altitude locations, at MSA were detected most of the SDE (85 %), whereas at MSY, with a larger exposure to anthropogenic pollutants, the detection of SDEs depended mainly on the intensity of the Saharan dust outbreak. At the MSY site 50 % of SDEs were detected, which were unequivocally identified when the relative contribution of mineral dust to PM_{10} was higher than 60 %.

The proximity to anthropogenic sources of mainly fine particles can prevent both the Ångström matrix and the SSAAE parameter from detecting SDEs. We have shown that transport of anthropogenic pollutants (mainly finer particles and precursors) from the urbanized/industrialized coastline towards regional areas inland can hinder the effect of mineral dust on the intensive aerosol optical properties during less intense SDEs. We have also shown that regional atmospheric scenarios occurring after SDEs may favour the recirculation of mineral dust at regional level in the WMB. Thus, mineral dust can remain in the atmosphere for a few days after the SDE. This fact is highly relevant for air quality since SDEs frequently promote exceedances in the PM_{10} daily limit value.

Thus, depending on the background atmospheric conditions, not all SDEs can be clearly detected using SAE, AAE and SSAAE parameters. Additional information provided, e.g. by forecast models, back-trajectory analysis and columnar measurements, is also required to better detect and characterize these events. Nevertheless, aethalometer and nephelometer instruments provide near-real-time measurements and allow a fast detection of the impact of SDEs at

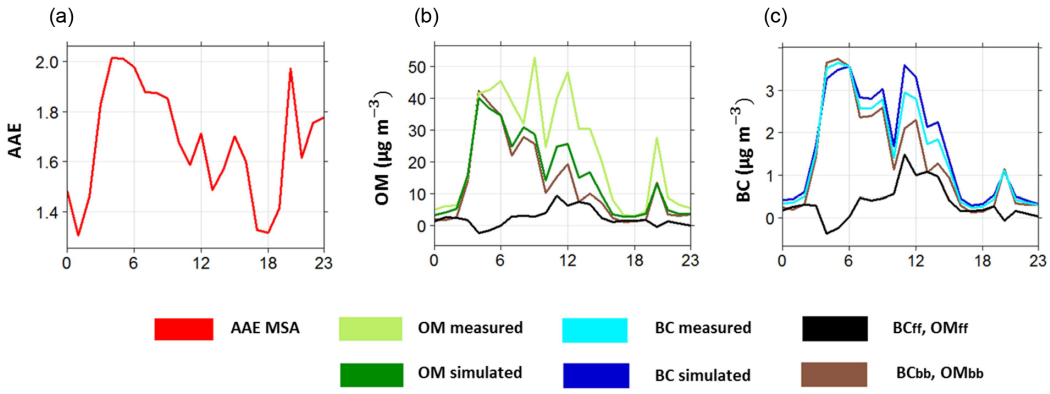

Figure 8. Daily cycle of **(a)** AAE, **(b)** Measured OM and simulated OM as the sum of OM_{ff} and OM_{bb} contributions, **(c)** Measured BC and simulated BC as the sum of BC_{ff} and BC_{bb} contributions, during a wildfire episode (23 July 2012) at MSY.

ground level. Furthermore, due to the sensitiveness for detecting changes in aerosol size and composition, SSAAE and Angstrom matrix tools are more sensitive compared to other near-real-time measurements.

A sensitivity test using the aethalometer model at MSY showed that the model constants, which are representative of the main emission sources, are actually site-dependent and should be calculated for the area under study. FF sources showed a larger contribution than BB at MSY, leading to $C_1 = 1.05$ and $C_2 = 0.26$ (g m^{-2}) for $AAE_{ff} = 1$ and $AAE_{bb} = 2$. Moreover C_3 was found to be significant mainly due to the large contribution of biogenic sources at MSY, showing values around 0.31 (µg m^{-3}). Linear relations were found for comparisons between OM_{bb} vs. BBOA ($R^2 = 0.43$) and OM_{ff} vs. HOA ($R^2 = 0.6$) showing fitting slopes of 1.27 and 4.4 respectively, which are consistent with SOA formation from BB and FF (25 and 90 %) emissions. Results from these comparisons were used to calibrate the aethalometer model, pointing to $AAE_{bb} = 2$ and $AAE_{ff} = 1$ as the most suitable values for our emplacement.

Annual averages of BC_{bb} contributions at MSY (36 %) and MSA (40 %) were significantly lower compared to other studies in northern Europe, due to less use of biomass burning as a heating system. OM_{bb} contributions accounted for 30 %. BB source contribution to both BC and OM were predominant during winter, with increasing AAE up to 1.5 when $\%BC_{bb}$ was higher than 50 %. Nevertheless, BC and OM were led by FF emissions sources during the summer period, due to stronger summer recirculation processes which are strengthened by sea and mountain breezes favouring the transport of pollutants toward regional areas inland. An interesting wildfire episode showed AAE values up to 2, accounting for BB contributions to BC and OM of 73 and 78 % respectively.

The aethalometer model is a powerful tool for reproducing long periods of real-time FF and BB contribution to BC, even in those areas where there is a predominance of carbonaceous material from non-combustion sources and BB emissions does not present very large contributions. BC, as the sum of BC_{ff} and BC_{bb}, was well reproduced showing a slight overestimation of 11 and 13 % at MSY and MSA. Results for BC_{ff} and BC_{bb} in winter and summer were in agreement with previous studies at MSY deployed by ^{14}C analysis. Furthermore, BC_{ff} and NO_2, both representative of traffic sources, showed good correlation for the winter period ($R^2 = 0.64$).

However, the model presents larger uncertainty concerning OM apportionment as reported in other studies (Favez et al., 2010; Herich et al., 2011). Biogenic sources, which present important contributions to our emplacement, are probably slightly underestimated by the model due to the partial apportionment of C_3 constant within OM_{ff} and OM_{bb}. Furthermore, OM_{bb} might be slightly overestimated due to the account of anthropogenic SOA within it, which can overlap with the absorption in the UV range. Despite the uncertainties associated with the source apportionment technique, OM time variation appears to be well reproduced. Nevertheless, OM formation and transformation processes occurring in the NWM should be taken into account when performing the AE model results, where important photochemical reactions take place led by large anthropogenic emissions and high insolation (mainly in summer).

The differentiation of brown carbon originated from different emission sources by using optical measurements is a challenge, in particular the SOA formation and transformation processes. Due to the uncertainties presented by the aethalometer model for providing absolute concentrations, it is recommended to carry out simultaneous measurements/experiments, applying different techniques not based on optical methods, such as using levoglucosan as a BB tracer or calibrating the model with BBOA obtained from ACSM source apportionment in order to assess the quantification of biomass burning by the model. Nevertheless, the aethalometer model is a very useful tool which provides satisfactory estimations of the temporal variability of the contributions for both biomass burning and fossil fuel emission sources. Further research in characterizing brown carbon by

means of optical techniques is needed to exploit the possibilities of the instrument.

The nephelometer and aethalometer instruments are widely used within monitoring networks and present several advantages for near-real-time air-quality monitoring at high temporal resolution. We have demonstrated the potential of the intensive optical parameters obtained from both instruments for detecting specific air pollution scenarios in near real time. This is possible given the high sensitivity of particular intensive aerosol optical parameters to characterize different types of atmospheric aerosols. However, it is necessary to perform a previous sensitivity test in order to evaluate and calibrate the intensive optical properties for detecting specific pollution episodes at different emplacements.

7 Data availability

The Montseny and Montsec data sets used for this publication are accessible online on the WDCA (World Data Centre for Aerosols) web page: http://ebas.nilu.no.

The Supplement related to this article is available online at doi:10.5194/acp-16-12567-2016-supplement.

Acknowledgements. This work was supported by the MINECO (Spanish Ministry of Economy and Competitiveness), the MAGRAMA (Spanish Ministry of Agriculture, Food and Environment), the Generalitat de Catalunya (AGAUR 2014 SGR33 and the DGQA) and FEDER funds under the PRISMA project (CGL2012-39623-C02/00). This work has received funding from the European Union's Horizon 2020 research and innovation programme under grant agreement No 654109. Marco Pandolfi is funded by a Ramón y Cajal Fellowship (RYC-2013-14036) awarded by the Spanish Ministry of Economy and Competitiveness. The authors would like to express their gratitude to D. C. Carslaw and K. Ropkins for providing the OpenAir software used in this paper (Carslaw and Ropkins, 2012; Carslaw, 2012).

Edited by: N. Mihalopoulos
Reviewed by: three anonymous referees

References

Alastuey, A., Minguillón, M. C., Pérez, N., Querol, X., Viana, M., and de Leeuw, F.: PM_{10} measurement methods and correction factors: 2009 status report, ETC/ACM Technical Paper 2011/21, 2011.

Albrecht, B. A.: Aerosols, Cloud Microphysics, and Fractional Cloudiness, Science, 245, 1227–1230, doi:10.1126/science.245.4923.1227, 1989.

Alfaro, S. C., Lafon, S., Rajot, J. L., Formenti, P., Gaudichet, A., and Maillé, M.: Iron oxides and light absorption by pure desert dust: An experimental study, J. Geophys. Res., 109, D08208, doi:10.1029/2003JD004374, 2004.

Andreae, M. O. and Gelencsér, A.: Black carbon or brown carbon? The nature of light-absorbing carbonaceous aerosols, Atmos. Chem. Phys., 6, 3131–3148, doi:10.5194/acp-6-3131-2006, 2006.

Andrews, E., Sheridan, P. J., Fiebig, M., McComiskey, A., Ogren, J. A., Arnott, P., Covert, D., Elleman, R., Gasparini, R., Collins, D., Jonsson, H., Schmid, B., and Wang, J.: Comparison of methods for deriving aerosol asymmetry parameter, J. Geophys. Res., 111, D05S04, doi:10.1029/2004JD005734, 2006.

Andrews, E., Ogren, J. A., Bonasoni, P., Marinoni, A., Cuevas, E., Rodríguez, S., Sun, J. Y., Jaffe, D. A., Fischer, E. V., Baltensperger, U., Weingartner, E., Coen, M. C., Sharma, S., Macdonald, A. M., Leaitch, W. R., Lin, N.-H., Laj, P., Arsov, T., Kalapov, I., Jefferson, A., and Sheridan, P.: Climatology of aerosol radiative properties in the free troposphere, Atmos. Res., 102, 365–393, doi:10.1016/j.atmosres.2011.08.017, 2011.

Basart, S., Pérez, C., Nickovic, S., Cuevas, E., and Baldasano, J. M.: Development and evaluation of the BSC-DREAM8b dust regional model over Northern Africa, the Mediterranean and the Middle East, Tellus B, 64, 18539, doi:10.3402/tellusb.v64i0.18539, 2012.

Berkowitz, C. M., Berg, L. K., Yu, X.-Y., Alexander, M. L., Laskin, A., Zaveri, R. A., Jobson, B. T., Andrews, E., and Ogren, J. A.: The influence of fog and airmass history on aerosol optical, physical and chemical properties at Pt. Reyes National Seashore, Atmos. Environ., 45, 2559–2568, doi:10.1016/j.atmosenv.2011.02.016, 2011.

Bond, T. C., Doherty, S. J., Fahey, D. W., Forster, P. M., Berntsen, T., Deangelo, B. J., Flanner, M. G., Ghan, S., Kärcher, B., Koch, D., Kinne, S., Kondo, Y., Quinn, P. K., Sarofim, M. C., Schultz, M. G., Schulz, M., Venkataraman, C., Zhang, H., Zhang, S., Bellouin, N., Guttikunda, S. K., Hopke, P. K., Jacobson, M. Z., Kaiser, J. W., Klimont, Z., Lohmann, U., Schwarz, J. P., Shindell, D., Storelvmo, T., Warren, S. G., and Zender, C. S.: Bounding the role of black carbon in the climate system: A scientific assessment, J. Geophys. Res.-Atmos., 118, 5380–5552, doi:10.1002/jgrd.50171, 2013.

Chen, Y. and Bond, T. C.: Light absorption by organic carbon from wood combustion, Atmos. Chem. Phys., 10, 1773–1787, doi:10.5194/acp-10-1773-2010, 2010.

Collaud Coen, M., Weingartner, E., Schaub, D., Hueglin, C., Corrigan, C., Henning, S., Schwikowski, M., and Baltensperger, U.: Saharan dust events at the Jungfraujoch: detection by wavelength dependence of the single scattering albedo and first climatology analysis, Atmos. Chem. Phys., 4, 2465–2480, doi:10.5194/acp-4-2465-2004, 2004.

Collaud Coen, M., Weingartner, E., Apituley, A., Ceburnis, D., Fierz-Schmidhauser, R., Flentje, H., Henzing, J. S., Jennings, S. G., Moerman, M., Petzold, A., Schmid, O., and Baltensperger, U.: Minimizing light absorption measurement artifacts of the Aethalometer: evaluation of five correction algorithms, Atmos. Meas. Tech., 3, 457–474, doi:10.5194/amt-3-457-2010, 2010.

Crippa, M., DeCarlo, P. F., Slowik, J. G., Mohr, C., Heringa, M. F., Chirico, R., Poulain, L., Freutel, F., Sciare, J., Cozic, J., Di Marco, C. F., Elsasser, M., Nicolas, J. B., Marchand, N., Abidi,

E., Wiedensohler, A., Drewnick, F., Schneider, J., Borrmann, S., Nemitz, E., Zimmermann, R., Jaffrezo, J.-L., Prévôt, A. S. H., and Baltensperger, U.: Wintertime aerosol chemical composition and source apportionment of the organic fraction in the metropolitan area of Paris, Atmos. Chem. Phys., 13, 961–981, doi:10.5194/acp-13-961-2013, 2013.

Cubison, M. J., Ortega, A. M., Hayes, P. L., Farmer, D. K., Day, D., Lechner, M. J., Brune, W. H., Apel, E., Diskin, G. S., Fisher, J. A., Fuelberg, H. E., Hecobian, A., Knapp, D. J., Mikoviny, T., Riemer, D., Sachse, G. W., Sessions, W., Weber, R. J., Weinheimer, A. J., Wisthaler, A., and Jimenez, J. L.: Effects of aging on organic aerosol from open biomass burning smoke in aircraft and laboratory studies, Atmos. Chem. Phys., 11, 12049–12064, doi:10.5194/acp-11-12049-2011, 2011.

Cusack, M., Alastuey, A., Pérez, N., Pey, J., and Querol, X.: Trends of particulate matter ($PM_{2.5}$) and chemical composition at a regional background site in the Western Mediterranean over the last nine years (2002–2010), Atmos. Chem. Phys., 12, 8341–8357, doi:10.5194/acp-12-8341-2012, 2012.

Delene, D. J. and Ogren, J. A.: Variability of aerosol optical properties at four North American surface monitoring sites, J. Atmos. Sci., 59, 1135–1149, 2002.

Draxler, R. R. and Rolph, G. D.: HYSPLIT (HYbrid Single-Particle Lagrangian Integrated Trajectory) Model access via NOAA ARL READY Website, available at: http://ready.arl.noaa.gov/HYSPLIT.php, NOAA Air Resources Laboratory, Silver Spring, MD, 2015.

Drinovec, L., Mocnik, G., Zotter, P., Prévôt, A. S. H., Ruckstuhl, C., Coz, E., Rupakheti, M., Sciare, J., Müller, T., Wiedensohler, A., and Hansen, A. D. A.: The "dual-spot" Aethalometer: an improved measurement of aerosol black carbon with real-time loading compensation, Atmos. Meas. Tech., 8, 1965–1979, doi:10.5194/amt-8-1965-2015, 2015.

Escudero, M., Querol, X., Ávila, A., and Cuevas, E.: Origin of the exceedances of the European daily PM limit value in regional background areas of Spain, Atmos. Environ., 41, 4, 730–744, doi:10.1016/j.atmosenv.2006.09.014, 2007a.

Escudero, M., Querol, X., Pey, J., Alastuey, A., Pérez, N., Ferreira, F., Alonso, S., Rodríguez, S., and Cuevas, E.: A methodology for the quantification of the net African dust load in air quality monitoring networks, Atmos. Environ., 41, 5516–5524, doi:10.1016/j.atmosenv.2007.04.047, 2007b.

Favez, O., El Haddad, I., Piot, C., Boréave, A., Abidi, E., Marchand, N., Jaffrezo, J.-L., Besombes, J.-L., Personnaz, M.-B., Sciare, J., Wortham, H., George, C., and D'Anna, B.: Inter-comparison of source apportionment models for the estimation of wood burning aerosols during wintertime in an Alpine city (Grenoble, France), Atmos. Chem. Phys., 10, 5295–5314, doi:10.5194/acp-10-5295-2010, 2010.

Garcia-Hurtado, E., Pey, J., Borrás, E., Sánchez, P., Vera, T., Carratalá, A., Alastuey, A., Querol, X., and Vallejo, V. R.: Atmospheric PM and volatile organic compounds released from Mediterranean shrubland wildfires, Atmos. Environ., 89, 85–92, doi:10.1016/j.atmosenv.2014.02.016, 2014.

Harrison, R. M., Beddows, D. C. S., Jones, A. M., Calvo, A., Alves, C., and Pio, C.: An evaluation of some issues regarding the use of aethalometers to measure woodsmoke concentrations, Atmos. Environ., 80, 540–548, doi:10.1016/j.atmosenv.2013.08.026, 2013.

Herich, H., Hueglin, C., and Buchmann, B.: A 2.5 year's source apportionment study of black carbon from wood burning and fossil fuel combustion at urban and rural sites in Switzerland, Atmos. Meas. Tech., 4, 1409–1420, doi:10.5194/amt-4-1409-2011, 2011.

IPCC: Climate Change 2007: The Physical Science Basis (Contribution ofWorking Group I to the Fourth Assessment Report of the Intergovernmental Panel on Climate Change), edited by: Solomon, S., Qin, D. Manning, M., Chen, Z., Marquis, M., Averyt, K. B., Tignor, M., and Miller, H. L., Cambridge Univ. Press, New York, USA, 131–217, 2007.

IPCC: Climate Change 2013: The Physical Science Basis. Working Group I contribution to the IPCC fifth assessment report, Final Draft Underlying Scientific-Technical Assessment, Cambridge University Press, Cambridge, United Kingdom and New York, NY, USA, 2013.

Jacobson, M. Z.: Studying the effects of aerosols on vertical photolysis rate coefficient and temperature profiles over an urban airshed, J. Geophys. Res., 103, 10593, doi:10.1029/98JD00287, 1998.

Jacobson, M. Z.: Global direct radiative forcing due to multicomponent anthropogenic and natural aerosols, J. Geophys. Res., 106, 1551, doi:10.1029/2000JD900514, 2001.

Jiménez, P., Lelieveld, J., and Baldasano, J. M.: Multiscale modeling of air pollutants dynamics in the northwestern Mediterranean basin during a typical summertime episode, J. Geophys. Res., 111, D18306, doi:10.1029/2005JD006516, 2006.

Jorba, O., Pandolfi, M., Spada, M., Baldasano, J. M., Pey, J., Alastuey, A., Arnold, D., Sicard, M., Artiñano, B., Revuelta, M. A., and Querol, X.: Overview of the meteorology and transport patterns during the DAURE field campaign and their impact to PM observations, Atmos. Environ., 77, 607–620, doi:10.1016/j.atmosenv.2013.05.040, 2013.

Kim, J., Bauer, H., Dobovicnik, T., Hitzenberger, R., Lottin, D., Ferry, D., and Petzold, A.: Constraining optical properties and refractive index of soot through combined experimental and modelling studies, European Aerosol Conference (EAC), Granada, Spain, 2–7 September 2012, Paper A-WG01S1P04, 2012.

Kirchstetter, T. W., Novakov, T., and Hobbs, P. V.: Evidence that the spectral dependence of light absorption by aerosols is affected by organic carbon, J. Geophys. Res.-Atmos., 109, 1–12, doi:10.1029/2004JD004999, 2004.

Laj, P., Klausen, J., Bilde, M., Plaß-Duelmer, C., Pappalardo, G., Clerbaux, C., Baltensperger, U., Hjorth, J., Simpson, D., Reimann, S., Coheur, P. F., Richter, A., De Mazière, M., Rudich, Y., McFiggans, G., Torseth, K., Wiedensohler, A., Morin, S., Schulz, M., Allan, J. D., Attié, J. L., Barnes, I., Birmili, W., Cammas, J. P., Dommen, J., Dorn, H. P., Fowler, D., Fuzzi, S., Glasius, M., Granier, C., Hermann, M., Isaksen, I. S. A, Kinne, S., Koren, I., Madonna, F., Maione, M., Massling, A., Moehler, O., Mona, L., Monks, P. S., Müller, D., Müller, T., Orphal, J., Peuch, V. H., Stratmann, F., Tanré, D., Tyndall, G., Abo Riziq, A., Van Roozendael, M., Villani, P., Wehner, B., Wex, H., and Zardini, A. A.: Measuring atmospheric composition change, Atmos. Environ., 43, 5351–5414, doi:10.1016/j.atmosenv.2009.08.020, 2009.

Laskin, A., Laskin, J., and Nizkorodov, S. A.: Chemistry of Atmospheric Brown Carbon, Chem. Rev., 115, 4335–4382, doi:10.1021/cr5006167, 2015.

Lewis, K., Arnott, W. P., Moosmüller, H., and Wold, C. E.: Strong spectral variation of biomass smoke light absorption and single scattering albedo observed with a novel dual-wavelength photoacoustic instrument, J. Geophys. Res., 113, D16203, doi:10.1029/2007JD009699, 2008.

Mallet, M., Dubovik, O., Nabat, P., Dulac, F., Kahn, R., Sciare, J., Paronis, D., and Léon, J. F.: Absorption properties of Mediterranean aerosols obtained from multi-year ground-based remote sensing observations, Atmos. Chem. Phys., 13, 9195–9210, doi:10.5194/acp-13-9195-2013, 2013.

Marcq, S., Laj, P., Roger, J. C., Villani, P., Sellegri, K., Bonasoni, P., Marinoni, A., Cristofanelli, P., Verza, G. P., and Bergin, M.: Aerosol optical properties and radiative forcing in the high Himalaya based on measurements at the Nepal Climate Observatory-Pyramid site (5079 m a.s.l.), Atmos. Chem. Phys., 10, 5859–5872, doi:10.5194/acp-10-5859-2010, 2010.

Millán, M. M., Salvador, R., Mantilla, E., and Kallos, G.: Photooxidant dynamics in the Mediterranean basin in summer: Results from European research projects, J. Geophys. Res., 102, 8811, doi:10.1029/96JD03610, 1997.

Minguillón, M. C., Perron, N., Querol, X., Szidat, S., Fahrni, S. M., Alastuey, A., Jimenez, J. L., Mohr, C., Ortega, A. M., Day, D. A., Lanz, V. A., Wacker, L., Reche, C., Cusack, M., Amato, F., Kiss, G., Hoffer, A., Decesari, S., Moretti, F., Hillamo, R., Teinilä, K., Seco, R., Peñuelas, J., Metzger, A., Schallhart, S., Müller, M., Hansel, A., Burkhart, J. F., Baltensperger, U., and Prévôt, A. S. H.: Fossil versus contemporary sources of fine elemental and organic carbonaceous particulate matter during the DAURE campaign in Northeast Spain, Atmos. Chem. Phys., 11, 12067–12084, doi:10.5194/acp-11-12067-2011, 2011.

Minguillón, M. C., Ripoll, A., Pérez, N., Prévôt, A. S. H., Canonaco, F., Querol, X., and Alastuey, A.: Chemical characterization of submicron regional background aerosols in the western Mediterranean using an Aerosol Chemical Speciation Monitor, Atmos. Chem. Phys., 15, 6379–6391, doi:10.5194/acp-15-6379-2015, 2015.

Mohr, C., DeCarlo, P. F., Heringa, M. F., Chirico, R., Slowik, J. G., Richter, R., Reche, C., Alastuey, A., Querol, X., Seco, R., Peñuelas, J., Jiménez, J. L., Crippa, M., Zimmermann, R., Baltensperger, U., and Prévôt, A. S. H.: Identification and quantification of organic aerosol from cooking and other sources in Barcelona using aerosol mass spectrometer data, Atmos. Chem. Phys., 12, 1649–1665, doi:10.5194/acp-12-1649-2012, 2012.

Moosmüller, H. and Chakrabarty, R. K.: Technical Note: Simple analytical relationships between Ångström coefficients of aerosol extinction, scattering, absorption, and single scattering albedo, Atmos. Chem. Phys., 11, 10677–10680, doi:10.5194/acp-11-10677-2011, 2011.

Müller, T., Henzing, J. S., de Leeuw, G., Wiedensohler, A., Alastuey, A., Angelov, H., Bizjak, M., Collaud Coen, M., Engström, J. E., Gruening, C., Hillamo, R., Hoffer, A., Imre, K., Ivanow, P., Jennings, G., Sun, J. Y., Kalivitis, N., Karlsson, H., Komppula, M., Laj, P., Li, S.-M., Lunder, C., Marinoni, A., Martins dos Santos, S., Moerman, M., Nowak, A., Ogren, J. A., Petzold, A., Pichon, J. M., Rodriquez, S., Sharma, S., Sheridan, P. J., Teinilä, K., Tuch, T., Viana, M., Virkkula, A., Weingartner, E., Wilhelm, R., and Wang, Y. Q.: Characterization and intercomparison of aerosol absorption photometers: result of two intercomparison workshops, Atmos. Meas. Tech., 4, 245–268, doi:10.5194/amt-4-245-2011, 2011a.

Müller, T., Laborde, M., Kassell, G., and Wiedensohler, A.: Design and performance of a three-wavelength LED-based total scatter and backscatter integrating nephelometer, Atmos. Meas. Tech., 4, 1291–1303, doi:10.5194/amt-4-1291-2011, 2011b.

Nickovic, S., Kallos, G., Papadopoulos, A., and Kakaliagou, O.: A model for prediction of desert dust cycle in the atmosphere, J. Geophys. Res., 106, 18113, doi:10.1029/2000JD900794, 2001.

Ogren, J. A., Andrews, E., McComiskey, A., Sheridan, P., Jefferson, A., and Fiebig, M.: New insights into aerosol asymmetry parameter, in: Proceedings of the 16th ARM Science Team Meeting, Albuquerque, NM, USA, 2006.

Pandolfi, M., Cusack, M., Alastuey, A., and Querol, X.: Variability of aerosol optical properties in the Western Mediterranean Basin, Atmos. Chem. Phys., 11, 8189–8203, doi:10.5194/acp-11-8189-2011, 2011.

Pandolfi, M., Ripoll, A., Querol, X., and Alastuey, A.: Climatology of aerosol optical properties and black carbon mass absorption cross section at a remote high-altitude site in the western Mediterranean Basin, Atmos. Chem. Phys., 14, 6443–6460, doi:10.5194/acp-14-6443-2014, 2014a.

Pandolfi, M., Querol, X., Alastuey, A., Jimenez, J. L., Jorba, O., Day, D., Ortega, A., Cubison, M. J., Comerón, A., Sicard, M., Mohr, C., Prévôt, A. S. H., Minguillón, M. C., Pey, J., Baldasano, J. M., Burkhart, J. F., Seco, R., Peñuelas, J., van Drooge, B. L., Artiñano, B., Di Marco, C., Nemitz, E., Schallhart, S., Metzger, A., Hansel, A., Lorente, J., Ng, S., Jayne, J., and Szidat, S.: Effects of sources and meteorology on particulate matter in the Western Mediterranean Basin: An overview of the DAURE campaign, J. Geophys. Res.-Atmos., 119, 4978–5010, doi:10.1002/2013JD021079, 2014b.

Pérez, C., Sicard, M., Jorba, O., Comerón, A., and Baldasano, J. M.: Summertime re-circulations of air pollutants over the northeastern Iberian coast observed from systematic EARLINET lidar measurements in Barcelona, Atmos. Environ., 38, 3983–4000, doi:10.1016/j.atmosenv.2004.04.010, 2004.

Pérez, N., Pey, J., Castillo, S., Viana, M., Alastuey, A., and Querol, X.: Interpretation of the variability of levels of regional background aerosols in the Western Mediterranean, Sci. Total Environ., 407, 527–540, doi:10.1016/j.scitotenv.2008.09.006, 2008.

Petzold, A. and Schönlinner, M.: Multi-angle absorption photometry – a new method for the measurement of aerosol light absorption and atmospheric black carbon, J. Aerosol Sci., 35, 421–441, doi:10.1016/j.jaerosci.2003.09.005, 2004.

Petzold, A., Rasp, K., Weinzierl, B., Esselborn, M., Hamburguer, T., Dörnbrack, A., Kandler, K., Schütz, L., Knippertz, P., Fiebig, M., and Virkkula, A.: Saharan dust absorption and refractive index from aircraft-based observations during SAMUM 2006, Tellus B, 61, 118–130, doi:10.1111/j.1600-0889.2008.00383.x, 2009.

Petzold, A., Ogren, J. A., Fiebig, M., Laj, P., Li, S.-M., Baltensperger, U., Holzer-Popp, T., Kinne, S., Pappalardo, G., Sugimoto, N., Wehrli, C., Wiedensohler, A., and Zhang, X.-Y.: Recommendations for reporting "black carbon" measurements, Atmos. Chem. Phys., 13, 8365–8379, doi:10.5194/acp-13-8365-2013, 2013.

Pey, J., Pérez, N., Querol, X., Alastuey, A., Cusack, M., and Reche, C.: Intense winter atmospheric pollution episodes affecting the

Western Mediterranean., Sci. Total Environ., 408, 1951–1959, doi:10.1016/j.scitotenv.2010.01.052, 2010.

Pey, J., Querol, X., Alastuey, A., Forastiere, F., and Stafoggia, M.: African dust outbreaks over the Mediterranean Basin during 2001–2011: PM_{10} concentrations, phenomenology and trends, and its relation with synoptic and mesoscale meteorology, Atmos. Chem. Phys., 13, 1395–1410, doi:10.5194/acp-13-1395-2013, 2013a.

Pey, J., Pérez, N., Cortés, J., Alastuey, A., and Querol, X.: Chemical fingerprint and impact of shipping emissions over a western Mediterranean metropolis: primary and aged contributions., Sci. Total Environ., 463–464, 497–507, doi:10.1016/j.scitotenv.2013.06.061, 2013b.

Pope, C. A. and Dockery, D. W.: Health effects of fine particulate air pollution: lines that connect, J. Air Waste Ma., 56, 709–42, 2006.

Querol, X., Pey, J., Pandolfi, M., Alastuey, A., Cusack, M., Pérez, N., Moreno, T., Viana, M., Mihalopoulos, N., Kallos, G., and Kleanthous, S.: African dust contributions to mean ambient PM_{10} mass-levels across the Mediterranean Basin, Atmos. Environ., 43, 4266–4277, doi:10.1016/j.atmosenv.2009.06.013, 2009.

Ramanathan, V. and Carmichael, G.: Global and regional climate changes due to black carbon, Nat. Geosci., 1, 221–227, doi:10.1038/ngeo156, 2008.

Reche, C., Viana, M., Amato, F., Alastuey, A., Moreno, T., Hillamo, R., Teinilä, K., Saarnio, K., Seco, R., Peñuelas, J., Mohr, C., Prévôt, A. S. H., and Querol, X.: Biomass burning contributions to urban aerosols in a coastal Mediterranean City, Sci. Total Environ., 427–428, 175–190, doi:10.1016/j.scitotenv.2012.04.012, 2012.

Ripoll, A., Pey, J., Minguillón, M. C., Pérez, N., Pandolfi, M., Querol, X., and Alastuey, A.: Three years of aerosol mass, black carbon and particle number concentrations at Montsec (southern Pyrenees, 1570 m a.s.l.), Atmos. Chem. Phys., 14, 4279–4295, doi:10.5194/acp-14-4279-2014, 2014.

Ripoll, A., Minguillón, M. C., Pey, J., Pérez, N., Querol, X., and Alastuey, A.: Joint analysis of continental and regional background environments in the western Mediterranean: PM_1 and PM_{10} concentrations and composition, Atmos. Chem. Phys., 15, 1129–1145, doi:10.5194/acp-15-1129-2015, 2015.

Rodríguez, S., Querol, X., Alastuey, A., Kallos, G., and Kakaliagou, O.: Saharan dust contributions to PM_{10} and TSP levels in Southern and Eastern Spain, Atmos. Environ., 35, 2433–2447, doi:10.1016/S1352-2310(00)00496-9, 2001.

Rodríguez, S., Querol, X., Alastuey, A., and Plana, F.: Sources and processes affecting levels and composition of atmospheric aerosol in the western Mediterranean, J. Geophys. Res., 107, 4777, doi:10.1029/2001JD001488, 2002.

Rodríguez, S., Querol, X., Alastuey, A., Viana, M.-M., and Mantilla, E.: Events Affecting Levels and Seasonal Evolution of Airborne Particulate Matter Concentrations in the Western Mediterranean, Environ. Sci. Technol., 37, 216–222, doi:10.1021/es020106p, 2003.

Rodríguez, S., Alastuey, A., Alonso-Pérez, S., Querol, X., Cuevas, E., Abreu-Afonso, J., Viana, M., Pérez, N., Pandolfi, M., and de la Rosa, J.: Transport of desert dust mixed with North African industrial pollutants in the subtropical Saharan Air Layer, Atmos. Chem. Phys., 11, 6663–6685, doi:10.5194/acp-11-6663-2011, 2011.

Rodríguez, S., Cuevas, E., Prospero, J. M., Alastuey, A., Querol, X., López-Solano, J., García, M. I., and Alonso-Pérez, S.: Modulation of Saharan dust export by the North African dipole, Atmos. Chem. Phys., 15, 7471–7486, doi:10.5194/acp-15-7471-2015, 2015.

Rolph, G. D.: Real-time Environmental Applications and Display system (READY) Website, available at: http://ready.arl.noaa.gov, NOAA Air Resources Laboratory, Silver Spring, MD, 2015.

Russell, P. B., Bergstrom, R. W., Shinozuka, Y., Clarke, A. D., DeCarlo, P. F., Jimenez, J. L., Livingston, J. M., Redemann, J., Dubovik, O., and Strawa, A.: Absorption Angstrom Exponent in AERONET and related data as an indicator of aerosol composition, Atmos. Chem. Phys., 10, 1155–1169, doi:10.5194/acp-10-1155-2010, 2010.

Sandradewi, J., Prévôt, A. S. H., Szidat, S., Perron, N., Alfarra, M. R., Lanz, V. A., Weingartner, E., and Baltensperger, U.: Using Aerosol Light Absorption Measurements for the Quantitative Determination of Wood Burning and Traffic Emission Contributions to Particulate Matter, Environ. Sci. Technol., 42, 3316–3323, doi:10.1021/es702253m, 2008.

Schuster, G. L., Dubovik, O., and Holben, B. N.: Angstrom exponent and bimodal aerosol size distributions, J. Geophys. Res., 111, D07207, doi:10.1029/2005JD006328, 2006.

Seco, R., Peñuelas, J., Filella, I., Llusia, J., Schallhart, S., Metzger, A., Müller, M., and Hansel, A.: Volatile organic compounds in the western Mediterranean basin: urban and rural winter measurements during the DAURE campaign, Atmos. Chem. Phys., 13, 4291–4306, doi:10.5194/acp-13-4291-2013, 2013.

Segura, S., Estellés, V., Titos, G., Lyamani, H., Utrillas, M. P., Zotter, P., Prévôt, A. S. H., Mocnik, G., Alados-Arboledas, L., and Martínez-Lozano, J. A.: Determination and analysis of in situ spectral aerosol optical properties by a multi-instrumental approach, Atmos. Meas. Tech., 7, 2373–2387, doi:10.5194/amt-7-2373-2014, 2014.

Seinfeld, J. H. and Pandis, S. N.: Atmospheric Chemistry and Physics: From Air Pollution to Climate Change, John Wiley, Hoboken, N. J., 1326 pp., 1998.

Sokolik, I. N. and Toon, O. B.: Incorporation of mineralogical composition into models of the radiative properties of mineral aerosol from UV to IR wavelengths, J. Geophys. Res., 104, 9423, doi:10.1029/1998JD200048, 1999.

Steinbrecher, R., Smiatek, G., Köble, R., Seufert, G., Theloke, J., Hauff, K., Ciccioli, P., Vautard, R., and Curci, G.: Intra- and inter-annual variability of VOC emissions from natural and semi-natural vegetation in Europe and neighbouring countries, Atmos. Environ., 43, 1380–1391, doi:10.1016/j.atmosenv.2008.09.072, 2009.

Twomey, S. A., Piepgrass, M., and Wolfe, T. L.: An assessment of the impact of pollution on global cloud albedo, Tellus B, 36B, 356–366, doi:10.1111/j.1600-0889.1984.tb00254.x, 1984.

Valenzuela, A., Olmo, F. J., Lyamani, H., Antón, M., Titos, G., Cazorla, A., and Alados-Arboledas, L.: Aerosol scattering and absorption Angström exponents as indicators of dust and dust-free days over Granada (Spain), Atmos. Res., 154, 1–13, doi:10.1016/j.atmosres.2014.10.015, 2015.

Viana, M., Reche, C., Amato, F., Alastuey, A., Querol, X., Moreno, T., Lucarelli, F., Nava, S., Calzolai, G., Chiari, M., and Rico, M.: Evidence of biomass burning aerosols in the Barcelona ur-

ban environment during winter time, Atmos. Environ., 72, 81–88, doi:10.1016/j.atmosenv.2013.02.031, 2013.

Weingartner, E., Saathoff, H., Schnaiter, M., Streit, N., Bitnar, B., and Baltensperger, U.: Absorption of light by soot particles: Determination of the absorption coefficient by means of aethalometers, J. Aerosol Sci., 34, 1445–1463, doi:10.1016/S0021-8502(03)00359-8, 2003.

Yang, M., Howell, S. G., Zhuang, J., and Huebert, B. J.: Attribution of aerosol light absorption to black carbon, brown carbon, and dust in China – interpretations of atmospheric measurements during EAST-AIRE, Atmos. Chem. Phys., 9, 2035–2050, doi:10.5194/acp-9-2035-2009, 2009.